AIAA SciTech Forum
6-10 January 2020, Orlando, FL
AIAA Scitech 2020 Forum

10.2514/6.2020-1962

Geometric Formulation for the Dynamics of Monarch Butterfly with the Effects of Abdomen Undulation

Madhu K. Sridhar,* Chang-kwon Kang†
University of Alabama Huntsville, Huntsville AL, 35899

Taeyoung Lee‡
The George Washington University, Washington DC, 20052

This paper presents a geometric formulation of the dynamics of a flapping wing aerial vehicle and utilize it to study the flight dynamics of a Monarch butterfly. The proposed model is essentially articulated rigid bodies, where two wings and an abdomen are connected to a thorax via spherical joint. An intrinsic form of Lagrangian mechanics is developed to study the inertial effects of the relative rotation between each part. Next, a quasi-steady aerodynamic model is presented without relying on the common assumption that the flapping frequency is sufficiently large. Consequently, it is suitable to study the flight of a butterfly that is characterized by relatively large wings flapping in a lower frequency. The outcome of the proposed model is compared with the captured motion of a live Monarch butterfly. It is shown that the undulation of the abdomen increases the climb rate and the forward velocity, and the motion of Monarch butterfly yields a stable period orbit.

I. Introduction

The Monarch butterfly is one of the most popular butterfly species in North America with wings of around 4 cm featuring an easily recognizable black, orange, and white pattern. They exhibit remarkable flight characteristics [1], migrating annually from North America to Mexico - up to 4000 km [2–4], the longest flight range among insects [2, 5–7]. However, the physical mechanism enabling this long-range flight is not well understood. One theory is that the Monarchs benefit from their high-altitude flight. Monarchs butterflies fly at high-altitudes during migration (~1,250m) and overwinter (~3,000m) at high altitudes. At these altitudes, they can take advantage of the boundary layer of the earth to conserve energy. Furthermore, aerodynamic drag is proportional to air density, which decreases with altitude. A minimal aerodynamic drag is critical to enable the long-range migration, which is provided by flying at high altitudes. However, the lift is also expected to decrease with lower density at higher altitudes. Unlike airplanes, Monarchs must generate the propulsive forces with their flapping motion. How butterflies efficiently generate lift and fly during migration is one of the unsolved mysteries.

Compared to the wealth of research on the flight of insects such as flies [8, 9], bees [10, 11], dragonflies [12–16], or birds and bats [17], butterfly flight remains inadequately understood due to their many unique characteristics. Unlike most insects, the fore and hindwings of butterflies are relatively large and move in sync [18]. Butterflies are extremely evasive with agile maneuvers [19–22] and body undulations with closely coupled wing-body interaction [21, 23, 24]. In particular, the butterfly body exhibits considerable vertical oscillation during flight due to the instantaneous change in wing shape and inertia [23, 25], resulting in a "bumpy" flight trajectory. Flapping wings and body move in unison as reported in our earlier work [24], suggesting that the butterfly flight is an outcome of closely coupled wing-body interaction.

The main obstacle in discovering the long-range flight mechanisms in the Monarch flight is this highly coupled dynamics of the slowly flapping motion and the body. The large wings continuously rotate during flight, which is also affected by the body dynamics. Furthermore, the thorax of the Monarchs continuously pitches while their abdomen moves relative to the thorax during flight. As a consequence, most flight dynamic equations of motion and control schemes that have been derived in the literature cannot be used to study the butterfly flight. The conventional models exploit the large disparity in the time scales of wingbeat frequency and body dynamics assuming smaller insects such as fruit flies and bumblebees [26, 27]. Furthermore, many flapping wing dynamics models are based on the common

*Graduate Student, Mechanical and Aerospace Engineering, University of Alabama Huntsville, 301 Sparkman Dr, Huntsville AL 35899
†Assistant Professor, Mechanical and Aerospace Engineering, University of Alabama Huntsville, 301 Sparkman Dr, Huntsville AL 35899
‡Associate Professor, Mechanical and Aerospace Engineering, The George Washington University, 800 22nd st NW, Washington DC, 20052.

simplified formulation where the nonlinear time-varying flapping dynamics are transformed into linear time-invariant systems by considering small perturbations averaged over the period of flapping [28–31]. These approaches are not suitable to analyze the low-frequency flapping dynamics of Monarch butterflies.

A key open research question associated with the butterfly flight is the effects of dynamics on the power consumption. Whereas the pitching motion of smaller flying insects play a critical role in aerodynamic force generation [8, 17], most butterfly wings are structurally restricted from pitching [25]. Instead, it is presumed that the relatively large aerodynamic forces generated by the simple flapping wing motions affect the body attitude and vertical displacement, which alter the effective angle of attack and, hence, the flapping wing aerodynamics. As such, by adjusting the center of mass, a butterfly inspired ornithopter without a tail could fly forward passively without a feedback controller [25]. If the forward flight of butterflies were indeed passive, the power consumption is expected to be lower than an actively controlled flight. The power savings due to coupled wing-body motion can contribute to our understanding of the long-range Monarch migration [32], which, in turn, can inform the development of long-range micro flying robots. However, there are also reports that contradict these findings: butterfly's flight under periodic flapping motion is unstable because the butterfly cannot maintain its body pitch angle within a proper range [33, 34]. The motion of the abdomen had to be actively controlled to stabilize the butterfly flight [34].

The objective of this paper is to derive, validate, and analyze a dynamic model that can characterize the Monarch butterfly flight. We model a flapping wing aerial vehicle as articulated rigid bodies, where two wings and an abdomen are connected to a thorax via spherical joint. An intrinsic form of Lagrangian mechanics is developed to include and study the inertial effects of the relative rotation between each part. These are developed on the nonlinear configuration manifold in a global fashion such that large angle rotational maneuvers can be analyzed without singularities and ambiguities inherent to the common attitude parameterizations. Further, this yields an elegant, structured form of the equations of motion that can be easily utilized in stability analysis and controller design.

Next, to model the flapping wing aerodynamics, a quasi-steady blade element model is formulated without relying on the common assumption that the flapping frequency is sufficiently large. For butterfly flights, the aerodynamic forces generated by the wing vary along the spanwise direction as the velocity generated by the flapping is comparable to the velocity of the thorax. We find the expression for the angle of attack at each infinitesimal chord of the wing as a function of the wing kinematics and the rotation and translation of the body, and it is utilized to compute the aerodynamic forces and moments.

In short, the proposed dynamic model captures the unique characteristics of the butterfly flight dynamics where the flapping of large wings are coupled with the thorax and the abdomen undulation. More specifically, it can represent the effects of the mass distribution of the relatively large wing, the inertial coupling with the abdomen undulation, and the low frequency flapping aerodynamics coupled with the body motion.

Finally, the results of this model are compared to the detailed motion of the thorax, abdomen, and the pair of wings of freely flying Monarch butterflies. The live Monarch butterfly flight is measured using a motion-tracking system [24], and the corresponding wing kinematics and the body undulations are extracted. It is illustrated that the simulation results constructed from the measured wing kinematics are consistent with the experimental results. Further we perform several numerical simulations to study the butterfly flight dynamics. Our results show that the trajectory of the velocity asymptotically converges to a periodic orbit, suggesting that the flapping motion captured by the Monarch butterfly yields an asymptotically stable periodic solution. Furthermore, it is demonstrated that the abdomen undulation as measured by the live Monarch butterfly increases the forward flight velocity and the climb rate, against the other cases of fixed abdomen or undulation in the opposite phase. The role of abdomen undulation in the stability of attitude dynamics has been presented in [35]. The presented results suggest that the abdomen may have another desirable effects on the translational dynamics of butterfly flight.

II. Flapping Wing Aerial Vehicle Model for Butterfly

In this section, we present a flapping wing aerial vehicle model that may characterize the flight of a butterfly. It is composed of a head, a thorax, an abdomen, and two wings attached to the thorax via spherical joints. We assume that the head and the thorax are coagulated into a single rigid body, which is referred to as *body*. Also, we assume that hindwings move in unison with forewings.

Here we present a mathematical description for the kinematics of the proposed articulated rigid body model. Define an inertial frame $\mathcal{F}_I = \{\mathbf{i}_x, \mathbf{i}_y, \mathbf{i}_z\}$, where the third axis points downward, and the first two axes span the horizontal plane (Fig. 1). This is compatible to the NED (north-east-down) frame common in flight dynamics.

A. Body

Define the body-fixed frame $\mathcal{F}_B = \{\mathbf{b}_x, \mathbf{b}_y, \mathbf{b}_z\}$, whose origin is located at its mass center of the body (Fig. 1). Following the common convention in flight dynamics, the first axis points toward the head, the second axis point toward the right wing, and the third axis points toward the ventral (belly) side.

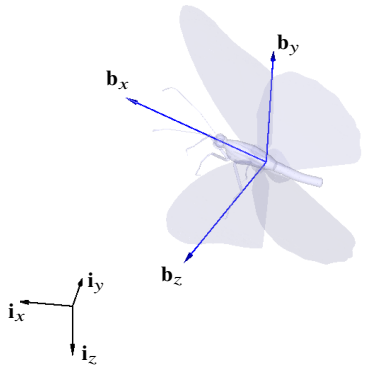

Fig. 1 The inertial frame $\mathcal{F}_I = \{\mathbf{i}_x, \mathbf{i}_y, \mathbf{i}_z\}$ (black) and the body-fixed frame $\mathcal{F}_B = \{\mathbf{b}_x, \mathbf{b}_y, \mathbf{b}_z\}$ (blue).

The location of the mass center of the body is given by $x \in \mathbb{R}^3$ in $\mathcal{F}_I$. The attitude of the body is described by $R \in \mathrm{SO}(3) = \{R \in \mathbb{R}^{3\times3} \mid R^T R = I_{3\times3},\ \det[R] = 1\}$, which represents the linear transformation of a representation of a vector from $\mathcal{F}_B$ to $\mathcal{F}_I$. The attitude kinematics is written as

$$\dot{R} = R\hat{\Omega}, \tag{1}$$

where $\Omega \in \mathbb{R}^3$ is the angular velocity resolved in $\mathcal{F}_B$. In the above equation, the *hat* map $\wedge : \mathbb{R}^3 \to \mathfrak{so}(3)$ is defined such that $\hat{x}y = x \times y$ for any $x, y \in \mathbb{R}^3$, or equivalently

$$\hat{x} = \begin{bmatrix} 0 & -x_3 & x_2 \\ x_3 & 0 & -x_1 \\ -x_2 & x_1 & 0 \end{bmatrix}, \tag{2}$$

for $x = (x_1, x_2, x_3) \in \mathbb{R}^3$. The inverse of the hat map is denoted by the *vee* map, $\vee : \mathfrak{so}(3) \to \mathbb{R}^3$.

B. Wing

Right Wing Let $\mathcal{F}_R = \{\mathbf{r}_x, \mathbf{r}_y, \mathbf{r}_z\}$ be the frame fixed to the right wing (Fig. 2). Its origin is located at the joint of the right wing, or the wing root where the right wing is attached to the thorax. The vector from the origin of $\mathcal{F}_B$ to the origin of $\mathcal{F}_R$ is defined as $\mu_R \in \mathbb{R}^3$. As it is resolved in $\mathcal{F}_B$ and the body is rigid, we have $\dot{\mu}_R = 0$. The first two axes of $\mathcal{F}_R$ span the plane of the wing, where the first axis points toward the leading edge and the second axis points toward the wing tip. Consequently, the third axis is normal to the wing plane, and it points toward the ventral side when there is no rotation of the right wing.

Next, we introduce the stroke frame $\mathcal{F}_S = \{\mathbf{s}_x, \mathbf{s}_y, \mathbf{s}_z\}$, which is constructed by translating the origin of $\mathcal{F}_B$ to the center of the left wing root and the right wing root, and rotating it about $\mathbf{b}_y$ by $\beta \in [-\pi, \pi)$ (Fig. 3). The y–z plane of $\mathcal{F}_S$ is referred to as the stroke plane.

The angle β can be considered as the angle between $\mathbf{b}_x$, and $\mathbf{s}_x$ that is normal to the stroke plane. Or equivalently, it is the angle between y–z plane of $\mathcal{F}_B$ and the stroke plane. It is positive when $\mathbf{s}_x \cdot \mathbf{b}_z < 0$. This angle is often defined as the angle between the ground (horizontal plane) and the stroke plane, considering hovering flights with a fixed attitude of the body. Here, it is defined relative to $\mathcal{F}_B$ as the flapping motion is inherently relative to the body.

The motion of the right wing relative to $\mathcal{F}_S$ is described by 1–3–2 Euler angles $(\phi_R, \psi_R, \theta_R)$ (Fig. 4). Consequently, the orientation of the right wing relative to $\mathcal{F}_B$, namely $Q_R \in \mathrm{SO}(3)$ is described by

$$Q_R(t) = \exp(\beta\hat{e}_2)\exp(\phi_R(t)\hat{e}_1)\exp(-\psi_R(t)\hat{e}_3)\exp(\theta_R(t)\hat{e}_2), \tag{3}$$

which is the linear transformation of a representation of a vector from $\mathcal{F}_R$ to $\mathcal{F}_B$. The Euler-angles are defined as

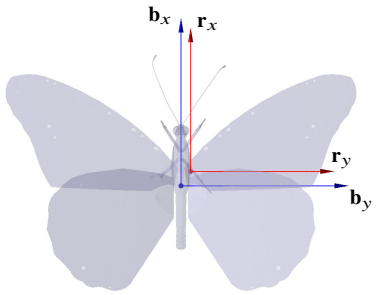

Fig. 2 The body-fixed frame $\mathcal{F}_B = \{\mathbf{b}_x, \mathbf{b}_y, \mathbf{b}_z\}$ (blue), the right wing frame $\mathcal{F}_R = \{\mathbf{r}_x, \mathbf{r}_y, \mathbf{r}_z\}$ (red)

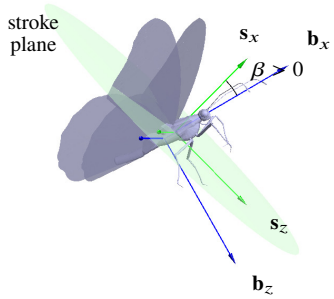

Fig. 3 The body-fixed frame $\mathcal{F}_B = \{\mathbf{b}_x, \mathbf{b}_y, \mathbf{b}_z\}$ (blue), the stroke frame $\mathcal{F}_S = \{\mathbf{s}_x, \mathbf{s}_y, \mathbf{s}_z\}$ (green).

$\phi_R \in [-\pi, \pi)$ the flapping angle, which is positive when the wing is in the ventral side, i.e., $\dot{\phi} > 0$ corresponds to downstroke and $\dot{\phi} < 0$ corresponds to upstroke (this is also referred to as the stroke angle or the sweep angle in other papers)

$\theta_R \in [-\pi, \pi)$ the pitch angle about the axis from the wing root to the wing tip, which is positive when the leading edge of the wing is rotated toward the dorsal side (this is also referred to as the feathering angle or the rotation angle in other papers)

$\psi_R \in [-\pi, \pi)$ the deviation angle that governs the motion of the wing tip out of the stroke plane, which is positive when the wing tip is rotated toward the head

As given by (3), the three-dimensional attitude of the right wing is parameterized by four angles, and as such there is a redundancy in defining the stroke plane. In general, the deviation angle is relatively small for most of insects. In particular, when ψ_R is exactly zero, the stroke plane is defined such that it is spanned by the motion of the wing tip. If the deviation angle is not zero, then the stroke plane can be chosen such that the distance between the wing tip and the

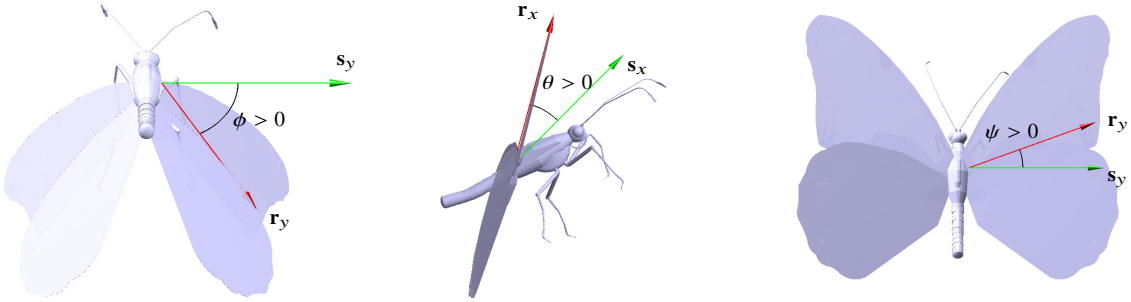

(a) flapping angle (b) pitch angle (c) deviation angle

Fig. 4 Wing configuration when only one of (ϕ, θ, ψ) is non-zero.

stroke plane, after integrated over a stroke, is minimized. This will be further discussed in Section V.

The time-derivative of Q_R is given by

$$\dot{Q}_R = Q_R \hat{\Omega}_R, \tag{4}$$

where $\Omega_R \in \mathbb{R}^3$ is the angular velocity of the right wing relative to $\mathcal{F}_B$ resolved in $\mathcal{F}_R$. One can show that the angular velocity of the right wing is obtained from the time-derivatives of the Euler-angles as

$$\Omega_R = \begin{bmatrix} \cos\psi_R \cos\theta_R & 0 & \sin\theta_R \\ \sin\psi_R & 1 & 0 \\ \cos\psi_R \sin\theta_R & 0 & -\cos\theta_R \end{bmatrix} \begin{bmatrix} \dot{\phi}_R \\ \dot{\theta}_R \\ \dot{\psi}_R \end{bmatrix}. \tag{5}$$

The determinant of the above 3×3 matrix is $-\cos\psi_R$. Consequently, it is invertible when the deviation angle satisfies $\psi_R \neq \pm\frac{\pi}{2}$. This is not restrictive as the deviation angle is small in general.

Left Wing Similarly, let $\mathcal{F}_L$ be the frame fixed to the left wing (Fig. 5). It can be obtained by translating $\mathcal{F}_R$ to the root of the left wing without any rotation. More specifically, its origin is located at the joint of the left wing, where the left wing is attached to the thorax. The first two axes span the plane of the wing, where the first axis points toward the leading edge and the second axis points toward the right wing, opposite to the left wing tip. Consequently, the third axis is normal to the wing plane, and it points toward the ventral side when there is no rotation of the left wing.

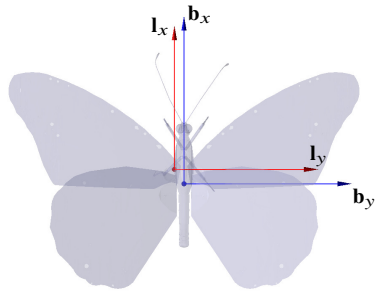

Fig. 5 The body-fixed frame $\mathcal{F}_B = \{\mathbf{b}_x, \mathbf{b}_y, \mathbf{b}_z\}$ (blue), the left wing frame $\mathcal{F}_L = \{\mathbf{l}_x, \mathbf{l}_y, \mathbf{l}_z\}$ (red).

Similar as the right wing, the motion of the left wing relative to the thorax is described by $Q_L \in \mathrm{SO}(3)$, which is described by successive rotations as

$$Q_L(t) = \exp(\beta\hat{e}_2)\exp(-\phi_L(t)\hat{e}_1)\exp(\psi_L(t)\hat{e}_3)\exp(\theta_L(t)\hat{e}_2), \tag{6}$$

where the definition of the Euler-angles $(\phi_L, \theta_L, \psi_L)$ are consistent with those of the right wing. The wing kinematics become symmetric when $(\phi_R, \theta_R, \psi_R) = (\phi_L, \theta_L, \psi_L)$.

The time-derivative of Q_L is given by

$$\dot{Q}_L = Q_L \hat{\Omega}_L, \tag{7}$$

where $\Omega_L \in \mathbb{R}^3$ is the angular velocity of the left wing relative to $\mathcal{F}_B$ resolved in $\mathcal{F}_L$. Also, we have

$$\Omega_L = \begin{bmatrix} -\cos\psi_L \cos\theta_L & 0 & -\sin\theta_L \\ \sin\psi_L & 1 & 0 \\ -\cos\psi_L \sin\theta_L & 0 & \cos\theta_L \end{bmatrix} \begin{bmatrix} \dot{\phi}_L \\ \dot{\theta}_L \\ \dot{\psi}_L \end{bmatrix}. \tag{8}$$

Wing Kinematics Let $f \in \mathbb{R}$ be the frequency of the flapping in Hz. Thus, the period of the flapping is $T = \frac{1}{f}$. The variation of the Euler angles over the flapping period is often referred to as wing kinematics, and several models have been presented to construct $(\phi(t), \theta(t), \psi(t))$ [36]. These can substituted into (3) and (6) to describe the attitude of the wing as a function of time.

C. Abdomen

Consider an abdomen that is assumed to be a rigid body attached to the thorax via a spherical joint. Let $\mathcal{F}_A = \{\mathbf{a}_x, \mathbf{a}_y, \mathbf{a}_z\}$ be the frame fixed to the abdomen. Its origin is located at the mass center of the abdomen, and its orientation is identical to $\mathcal{F}_B$ when there is no rotation relative to the body. The vector from the origin of $\mathcal{F}_B$ to the joint connecting the thorax and the abdomen is $\mu_A \in \mathbb{R}^3$. As it is resolved in $\mathcal{F}_B$ and the body is rigid, we have $\dot{\mu}_A = 0$.

The motion of the abdomen relative to the body is described by $Q_A \in \mathrm{SO}(3)$, which is the linear transformation of the representation of a vector from $\mathcal{F}_A$ to $\mathcal{F}_B$. Its time-derivative is given by

$$\dot{Q}_A = Q_A \hat{\Omega}_A, \tag{9}$$

where $\Omega_A \in \mathbb{R}^3$ is the angular velocity of the abdomen relative to the body, resolved in $\mathcal{F}_A$.

III. Quasi-Steady Aerodynamics

The quasi-steady assumption implies that the aerodynamic force and moment generated by the flapping wing are equivalent to those for steady motion at the same instantaneous velocity and the angle of attack. In this section, we propose a quasi-steady aerodynamic model for the butterfly flights characterized by relatively slow flapping of large wings. Without relying on the common assumption that the flapping frequency is sufficiently large, an expression for the translational forces and the rotational force is presented. This accounts the effects of the translational and rotational motion of the body, and the wind gust in the aerodynamic force.

A. Wing Morphological Parameters

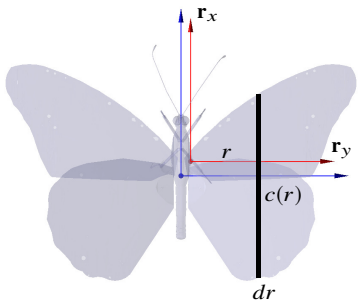

Fig. 6 Infinitesimal wing segment.

We first present several morphological parameters of the wing as formulated in to [37], after making a few changes in the notation. More specifically, in [37], the symbol $\wedge$ is used to denote normalized variables. However, the same symbol is used for the hat map in (2). Instead, we use the symbol $\tilde{}$ for the normalized variables to avoid conflict with (2). Also, the morphological parameters are defined for a single wing as the aerodynamic force of the left wing will be distinguished from the right wing for non-symmetric flapping.

Let dr be the infinitesimal wing segment located distanced at r from the wing root (Fig. 6). Let its chord be defined as $c(r)$. The wing segment is parallel to $\mathbf{r}_x$ and the distance is measured along $\mathbf{r}_y$. Assume that the aerodynamic center of the segment is along $\mathbf{r}_y$, i.e., the resultant force generated by the wing segment is located along $\mathbf{r}_y$ with zero moment. Consequently, it is located at re_2 when resolved in $\mathcal{F}_R$.

The area of the right wing is given by

$$S = \int_0^l c(r)dr, \tag{10}$$

where $l > 0$ is the wing span, i.e., the distance between the wing root and the wing tip measure along $\mathbf{r}_y$. The non-dimensional aspect ratio is

$$AR = \frac{l^2}{S}. \tag{11}$$

The mean chord is the area divided by the span, i.e., $\bar{c} = \frac{S}{l}$, and the normalized wing chord is

$$\tilde{c} = \frac{c}{\bar{c}} = \frac{cl}{S}. \tag{12}$$

Also, the non-dimensional radius is defined as

$$\tilde{r} = \frac{r}{l}. \tag{13}$$

The k-th moment of wing area is defined as

$$S_k = \int_0^l r^k c(r) dr = S l^k \int_0^1 \tilde{r}^k \tilde{c} d\tilde{r}, \tag{14}$$

satisfying $S_0 = S$. The non-dimensional radius of the k-th moment of wing area is defined as

$$\tilde{r}_k = \left(\frac{S_k}{S l^k}\right)^{\frac{1}{k}} = \left(\frac{1}{S l^k} \int_0^l r^k c(r) dr\right)^{\frac{1}{k}} = \left(\int_0^1 \tilde{r}^k \tilde{c} d\tilde{r}\right)^{\frac{1}{k}}, \tag{15}$$

such that $S_k = (\tilde{r}_k l)^k S$, i.e., if all of the wing area is located at a distance $\tilde{r}_k l$, the k-th moment of area is equal to S_k.

Next, when a wing is accelerated, it causes the motion of the surrounding air. The inertia of the wing is increased by the mass of air that is accelerated, and therefore there is an increase in the wing mass. The normalized virtual mass is defined as

$$\tilde{v} = \int_0^1 \tilde{c}^2 d\tilde{r}. \tag{16}$$

And the corresponding normalized radius of the k-th moment of virtual mass is

$$\tilde{r}_k(v) = \left(\frac{1}{\tilde{v}} \int_0^1 \tilde{c}^2 \tilde{r}^k d\tilde{r}\right)^{\frac{1}{k}}. \tag{17}$$

B. Blade-Element Theory

Angle of Attack of Right Wing When resolved in the inertial frame, the root of the right wing is located at $x + R\mu_R$. Thus, the aerodynamic center of the chord at the distance r from the wing root is

$$x + R\mu_R + RQ_R r e_2.$$

Therefore, its velocity in $\mathcal{F}_I$ is

$$\dot{x} + R\hat{\Omega}\mu_R + R\hat{\Omega}Q_R r e_2 + RQ_R\hat{\Omega}_R r e_2,$$

which is transformed to $\mathcal{F}_R$ by left-multiplying $Q_R^T R^T$ as

$$\begin{aligned} &Q_R^T R^T \dot{x} + Q_R^T \hat{\Omega}\mu_R + Q_R^T \hat{\Omega} Q_R r e_2 + \hat{\Omega}_R r e_2 \\ &\quad = Q_R^T (R^T \dot{x} + \Omega \times \mu_R) + r(Q_R\Omega + \Omega_R) \times e_2, \end{aligned}$$

where the first term corresponds to the velocity of the wing root and the second term corresponds to the velocity of the aerodynamic center relative to the wing root. Both are resolved in $\mathcal{F}_R$.

Assume that there is a uniform wind with the velocity $v_{\text{wind}} \in \mathbb{R}^3$ resolved in $\mathcal{F}_I$. The velocity of the aerodynamic center of $c(r)$ relative to the wind is given by

$$Q_R^T (R^T (\dot{x} - v_{\text{wind}}) + \Omega \times \mu_R) + r(Q_R\Omega + \Omega_R) \times e_2,$$

According to the *blade-element theory* [37], the aerodynamic force generated by the infinitesimal chord is independent of the span-wise velocity component, i.e., the component of the above expression along $\mathbf{r}_y$ is irrelevant. Therefore, we project the above velocity to the $\mathbf{r}_x$–$\mathbf{r}_z$ plane as follows.

$$U_R(r) = (I_{3\times3} - e_2 e_2^T) Q_R^T (R^T (\dot{x} - v_{\text{wind}}) + \Omega \times \mu_R) + r(Q_R\Omega + \Omega_R) \times e_2. \tag{18}$$

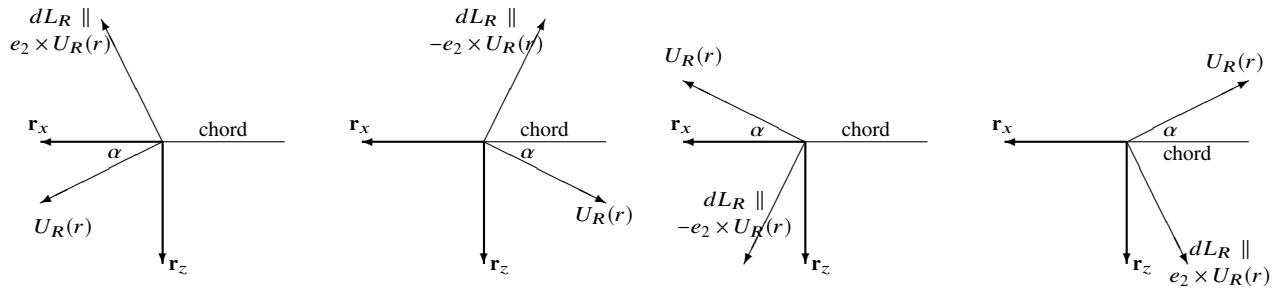

(a) Case 1 (b) Case 2 (c) Case 3 (d) Case 4

Fig. 7 Direction of the velocity and the lift in the $\mathbf{r}_x$–$\mathbf{r}_z$ plane of the right wing.

where $I_{3\times3} - e_2 e_2^T = \text{diag}[1, 0, 1] \in \mathbb{R}^{3\times3}$ corresponds to the projection operator. The second term is not affected by the projection as it is already normal to e_2. When the flapping frequency is sufficiently large, or equivalently Ω_R is relatively large compared with other terms, it can be simply approximated by $U_R(r) = r\Omega_R \times e_2$. But, the flapping frequency of a butterfly is about 10 Hz, and the contribution of the flapping to U_R is comparable to other terms caused by the body velocity.

The angle of attack $\alpha_R(r)$ is the angle between the chord line $\pm e_1$ and the above velocity $U_R(r)$. Assuming that the chord is a thin blade, when the angle is greater than $\frac{\pi}{2}$, we flip the leading edge and the trailing edge of the chord. This ensures that $\alpha_R(r) \in [0, \frac{\pi}{2}]$ always. More explicitly,

$$\alpha_R(r) = \cos^{-1}\left(\frac{|e_1^T U_R(r)|}{\|U_R(r)\|}\right). \tag{19}$$

The above expression has a singularity when $U(r) = 0$. But, the value of $\alpha(r)$ does not matter when $U(r) = 0$, as the resulting aerodynamic force and moment will vanish. Or equivalently, it can be written as

$$\alpha_R(r) = \sin^{-1}\left(\frac{|e_3^T U_R(r)|}{\|U_R(r)\|}\right). \tag{20}$$

Angle of Attack of Left Wing For the left wing, (18) is changed into

$$U_L(r) = (I_{3\times3} - e_2 e_2^T) Q_L^T (R^T(\dot{x} - v_{\text{wind}}) + \Omega \times \mu_L) - r(Q_L\Omega + \Omega_L) \times e_2. \tag{21}$$

The angle of attack is given by

$$\alpha_L(r) = \cos^{-1}\left(\frac{|e_1^T U_L(r)|}{\|U_L(r)\|}\right) = \sin^{-1}\left(\frac{|e_3^T U_L(r)|}{\|U_L(r)\|}\right). \tag{22}$$

C. Translational Forces

Right Wing Here we find the expression of the lift and the drag. The magnitude of the lift generated by the infinitesimal wing segment $c(r)$ is

$$\frac{1}{2}\rho\|U_R(r)\|^2 C_L(\alpha_R(r))c(r)dr,$$

where $\rho \in \mathbb{R}$ is the atmospheric density, and $C_L \in \mathbb{R}$ is the lift coefficient given as a function of the angle of attack.

The direction of the lift is normal to both of the velocity $U_R(r)$ and the wing span-wise direction e_2. As such, the direction of the lift is along $\pm e_2 \times U_R(r)$ in $\mathcal{F}_R$. The ambiguity of the sign can be resolved by the fact that when the $\mathbf{r}_x$–$\mathbf{r}_z$ plane is divided by the chord line $\mathbf{r}_x$, the velocity vector $U(r)$ and the lift vector occupy the opposite side with each other.

More specifically, consider the four cases illustrated in Fig. 7. These show that the direction of lift is $e_2 \times U_R(r)$ when $e_1^T U_R(r)$ and $e_3^T U_R(r)$ have the same sign (Case 1 and Case 4), and it is $-e_2 \times U_R(r)$ when they have the opposite sign (Case 2 and Case 3). Therefore, the infinitesimal lift vector resolved in $\mathcal{F}_R$ is given by

$$\begin{aligned} dL_R(r) &= \frac{1}{2}\rho U_R^2(r) C_L(\alpha(r)) c(r) \text{sgn}(e_1^T U_R(r) e_3^T U_R(r)) \frac{e_2 \times U_R(r)}{\|e_2 \times U(r)\|} dr \\ &= \frac{1}{2}\rho C_L(\alpha(r)) c(r) \text{sgn}(e_1^T U_R(r) e_3^T U_R(r)) (e_2 \times U_R(r)) \|U_R(r)\| dr, \end{aligned} \tag{23}$$

where the second equality is obtained by $\|U_R(r)\| = \|e_2 \times U_R(r)\|$.

The total lift of the right wing is obtained by integrating above span-wise for $r \in [0, l]$.

$$L_R = \int_0^l dL_R(r), \tag{24}$$

which is resolved in $\mathcal{F}_R$.

Next, the drag is always opposite to $U_R(r)$. Similar with the above expressions,

$$dD_R(r) = -\frac{1}{2}\rho C_D(\alpha(r)) c(r) \|U_R(r)\| U_R(r) dr. \tag{25}$$

The total drag is obtained by integrating above span-wise for $r \in [0, l]$ as

$$D_R = \int_0^l dD_R(r), \tag{26}$$

which is resolved in $\mathcal{F}_R$.

The lift and the drag also generate the moment about the wing root. When resolved in $\mathcal{F}_R$, it is given by

$$M_R = \int_0^l r e_2 \times (dL_R + dD_R). \tag{27}$$

Left Wing Similarly, the infinitesimal lift vector of the left wing resolved in $\mathcal{F}_L$ is given by

$$dL_L(r) = \frac{1}{2}\rho C_L(\alpha(r)) c(r) \text{sgn}(e_1^T U_L(r) e_3^T U_L(r)) (e_2 \times U_L(r)) \|U_L(r)\| dr, \tag{28}$$

which is integrated to obtain

$$L_L = \int_0^l dL_L(r). \tag{29}$$

Also, the infinitesimal drag of the left wing is

$$dD_L(r) = -\frac{1}{2}\rho C_D(\alpha(r)) c(r) \|U_L(r)\| U_L(r) dr, \tag{30}$$

and

$$D_L = \int_0^l dD_L(r), \tag{31}$$

which is resolved in $\mathcal{F}_R$.

The lift and the drag also generate the moment about the wing root as

$$M_L = \int_0^l -r e_2 \times (dL_L + dD_L). \tag{32}$$

D. Rotational Force

The wing's own rotation may cause additional circulation about the chord that generate a normal force. This is referred to as a rotational force [38]. The expression of the rotational force of the right wing is identical to that of the left wing, except the flipped sign in the corresponding moment. As such, in this section, we do not distinguish the right wing from the left wing with the subscript R.

According to [38], the magnitude of the rotational lift for the infinitesimal wing segment is given by

$$\rho\|U(r)\|C_{\text{rot}}|\dot{\alpha}(r)|c^2(r)dr, \tag{33}$$

where the last part $C_{\text{rot}}|\dot{\alpha}(R)|c^2$ corresponds to the rotational circulation. The time-derivative of the angle of attack multiplied by $\|U\|$ is given by

$$\begin{aligned}\|U\|\dot{\alpha} &= \frac{1}{\sin\alpha}\left\{\cos\alpha\frac{U^T\dot{U}}{\|U\|} - \text{sgn}(e_1^TU)(e_1^T\dot{U})\right\} \\ &= \frac{1}{\cos\alpha}\left\{-\sin\alpha\frac{U^T\dot{U}}{\|U\|} + \text{sgn}(e_3^TU)(e_3^T\dot{U})\right\}.\end{aligned} \tag{34}$$

To avoid singularity caused by α, the first expression is used when α is close to $\frac{\pi}{2}$, and the second expression is used when α is close to 0. Also, to mitigate the singularity caused by $\|U\| \ll 1$, we evaluate $\|U\|\dot{\alpha}$ in the numerical implementation, instead of computing $\dot{\alpha}$ directly.

Next, we find the direction of the rotational lift. It is shown that the rotational lift is always perpendicular to the chord line, and consequently it is $\pm e_3$ in $\mathcal{F}_R$. Consider the four cases of $\alpha > 0$ illustrated in Fig. 7. For the first two cases of $e_3^TU > 0$, $\dot{\alpha} > 0$ generates the rotational lift along $-e_3$, and for the last two cases of $e_3^TU(r) < 0$, $\dot{\alpha} > 0$ generates the rotational lift along e_3. Therefore, when $\alpha > 0$, the direction of the rotational lift is $-\text{sgn}(e_3^TU)\text{sgn}(\dot{\alpha})e_3$.

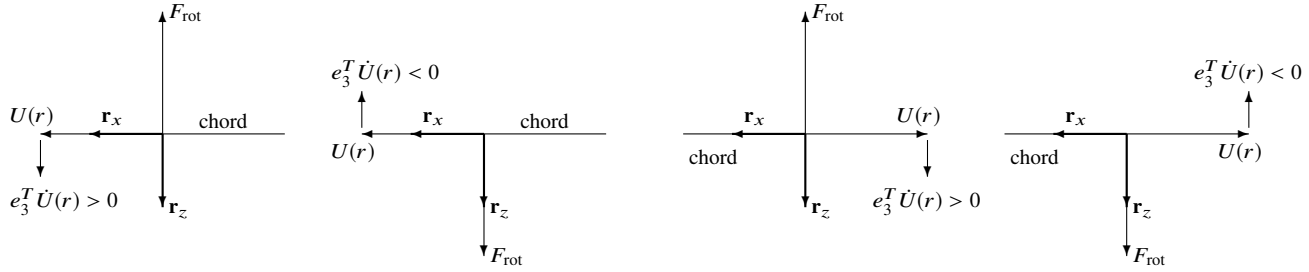

(a) Case 1 (b) Case 2 (c) Case 3 (d) Case 4

Fig. 8 Direction of the rotational lift when $\alpha = 0$ deg.

For the case of $\alpha = 0$, the direction of the rotational lift is illustrated in Fig. 8, where the rotational lift is always opposite to $e_3^T\dot{U}$. Therefore, its direction is given by $-\text{sgn}(e_3^T\dot{U})e_3$.

These two cases for the direction can be combined into

$$\text{sig}_{\text{rot}}(r)e_3, \tag{35}$$

where

$$\text{sig}_{\text{rot}} = \text{sgn}(\alpha(r))\{-\text{sgn}(e_3^TU(r))\text{sgn}(\dot{\alpha}(r))\} + (1 - \text{sgn}(\alpha(r)))\{-\text{sgn}(e_3^T\dot{U}(r))\}, \tag{36}$$

which takes the value of ± 1. Thus, the rotational lift vector is the product of the above direction and the magnitude (33).

$$dF_{\text{rot}} = \rho\|U(r)\|C_{\text{rot}}|\dot{\alpha}(r)|\text{sgn}_{\text{rot}}(r)e_3c^2(r)dr, \tag{37}$$

which is integrated to obtain the rotational force

$$F_{\text{rot}} = \int_0^l dF_{\text{rot}}. \tag{38}$$

For the right wing, the above rotational force generate the moment about the wing root as follows.

$$M_{\text{rot}_R} = \int_0^l re_2 \times dF_{\text{rot}},$$

which is resolved in $\mathcal{F}_R$. For the left wing, the chord is located at $-re_2$ in $\mathcal{F}_L$, and consequently

$$M_{\text{rot}_L} = -\int_0^l re_2 \times dF_{\text{rot}}.$$

IV. Dynamics of Flapping Wing Aerial Vehicle for Butterfly

In this section, we construct the equations of motion for the dynamics of the proposed flapping wing aerial vehicle model. To objective is to capture the inertial coupling between the thorax, the abdomen, and the wings such that the dynamics of butterfly is properly represented. It is based on the geometric formulation of the multibody dynamics [39] to describe the dynamics in an intrinsic, elegant fashion.

A. Lagrangian Mechanics on a Lie Group

We first present the Lagrangian mechanics for an arbitrary mechanical system evolving on a Lie group. The Euler–Lagrange equations are developed when the Lagrangian is composed of a kinetic energy with a configuration-dependent inertia and a potential energy. This result will be utilized later for the proposed flapping wing aerial vehicle.

Consider a dynamic system evolving on an abstract Lie group G. The kinematics equation on G is given by

$$\dot{g} = g\xi, \tag{39}$$

for $\xi \in \mathfrak{g}$ corresponding to the left-trivialized velocity. Consequently the tangent bundle TG is identified with $\mathsf{G} \times \mathfrak{g}$. Let $\mathbf{J} : \mathsf{G} \times \mathfrak{g} \to \mathfrak{g}^*$ be a symmetric, positive-definite inertia tensor, i.e.,

$$\begin{aligned}
\langle \mathbf{J}_g(\xi), \xi \rangle &\geq 0, \\
\langle \mathbf{J}_g(\xi), \xi \rangle = 0 &\;\Leftrightarrow\; \xi = 0, \\
\langle \mathbf{J}_g(\xi_1), \xi_2 \rangle &= \langle \mathbf{J}_g(\xi_2), \xi_1 \rangle,
\end{aligned}$$

for any $g \in \mathsf{G}$ and $\xi, \xi_1, \xi_2 \in \mathfrak{g}$. Also, define $(\mathbf{K}_g(\xi))(\cdot) : \mathsf{G} \times \mathfrak{g} \to \mathfrak{g}^*$ such that

$$\mathsf{T}_e^*\mathsf{L}_g \cdot \mathbf{D}_g\mathbf{J}_g(\xi) \cdot \chi = (\mathbf{K}_g(\xi))(\chi) = \mathbf{K}_g(\xi)\chi. \tag{40}$$

It is straightforward to $\mathbf{K}_g(\xi)$ is a linear operator. Therefore, by selecting a basis of $\mathfrak{g}$, $\mathbf{K}_g(\xi)$ can be represented by a matrix. Intuitively, it is the left-trivialize derivative of $\mathbf{J}_g(\xi)$ with respect to g.

Suppose that the Lagrangian $L : \mathsf{G} \times \mathfrak{g} \to \mathbb{R}$ is given by

$$L(g, \xi) = \frac{1}{2}\langle \mathbf{J}_g(\xi), \xi \rangle - U(g),$$

for a configuration dependent potential $U : \mathrm{SO}(3) \to \mathbb{R}$. We have

$$\begin{aligned}
\mathbf{D}_\xi L(g, \xi) &= \mathbf{J}_g(\xi), \\
\frac{d}{dt}\mathbf{D}_\xi L(g, \xi) &= \mathbf{J}_g(\dot{\xi}) + \mathbf{K}_g(\xi)\xi, \\
\mathsf{T}_e^*\mathsf{L}_g \cdot \mathbf{D}_g L(g, \xi) \cdot \chi &= \frac{1}{2}\langle \mathbf{K}_g(\xi)\chi, \xi \rangle - \mathsf{T}_e^*\mathsf{L}_g U(g) \cdot \chi \\
&= \left\{ \frac{1}{2}\mathbf{K}_g^*(\xi)\xi - \mathsf{T}_e^*\mathsf{L}_g U(g) \right\} \cdot \chi,
\end{aligned}$$

where $\mathfrak{g}^*$ is identified with $\mathfrak{g}$ with the pairing. Substituting these into [39, equation (8.45)], the Euler–Lagrange equations are given by

$$\mathbf{J}_g(\dot{\xi}) + \mathbf{K}_g(\xi)\xi - \mathrm{ad}_\xi^* \cdot \mathbf{J}_g(\xi) - \frac{1}{2}\mathbf{K}_g^*(\xi)\xi + \mathsf{T}_e^*\mathsf{L}_g U(g) = 0. \tag{41}$$

B. Lagrangian Mechanics of Flapping Wing Aerial Vehicle

The configuration of the given flapping wing vehicle model is described by $g = (x, R, Q_R, Q_L, Q_A)$. Consequently, the configuration space is a Lie group $\mathsf{G} = \mathbb{R}^3 \times \mathrm{SO}(3)^4$. As it is a product of $\mathbb{R}^3$ and four copies of SO(3), the Lie algebra is simply $\mathfrak{g} = \mathbb{R}^3 \times \mathfrak{so}(3)^4 \simeq \mathbb{R}^3 \times (\mathbb{R}^3)^4$. The kinematics equation is identical to (39) with $\xi = (\dot{x}, \Omega, \Omega_R, \Omega_L, \Omega_A) \in \mathfrak{g}$.

Kinetic Energy The kinetic energy of the body is given by

$$T_B = \frac{1}{2} m_B \|\dot{x}\|^2 + \frac{1}{2} \Omega^T J_B \Omega. \tag{42}$$

where $m_B \in \mathbb{R}$ is the mass of the body, and $J_B \in \mathbb{R}^{3\times3}$ is the inertia matrix of the body about $\mathcal{F}_B$.

Next, we find the expression for the kinetic energy of the wings and the abdomen. The contribution of the left wing is identical to the right wing and the abdomen, as all of them are essentially a rigid body connected to the thorax via a spherical joint. Therefore, we use the subscript $i \in \{R, L, A\}$ to denote the variables related to a particular wing or the abdomen, which is referred to as $\mathcal{B}_i$.

Consider a mass element dm in $\mathcal{B}_i$, whose location is given by $\nu \in \mathbb{R}^3$ in $\mathcal{F}_i$, i.e., ν is the vector from the joint to the mass element resolved in $\mathcal{F}_i$. Thus, its location from the origin of the inertial frame, resolved in the inertial frame $\mathcal{F}_I$ is $x + R\mu_i + RQ_i\nu$, and its velocity is

$$\dot{x} + R\hat{\Omega}(\mu_i + Q_i\nu) + RQ_i\hat{\Omega}_i\nu.$$

Therefore, the kinetic energy is

$$T_i = \frac{1}{2} \int_{\mathcal{B}_i} \frac{1}{2} \|\dot{x} + R\hat{\Omega}(\mu_i + Q_i\nu_i) + RQ_i\hat{\Omega}_i\nu_i\|^2 dm.$$

Let $m_i \in \mathbb{R}$ be the mass of $\mathcal{B}_i$, and let

$$\nu_i = \frac{1}{m_i} \int_{\mathcal{B}_i} \nu dm, \tag{43}$$

$$J_i = \int_{\mathcal{B}_i} \hat{\nu}^T \hat{\nu} dm. \tag{44}$$

Thus $\nu_i \in \mathbb{R}^3$ is the vector from the origin of $\mathcal{F}_i$ to the mass center of $\mathcal{B}_i$ resolved in $\mathcal{F}_i$, and $J_i \in \mathbb{R}^{3\times3}$ is the inertia matrix of $\mathcal{B}_i$ about the origin of $\mathcal{F}_i$ resolved in $\mathcal{F}_i$. After rearranging, one can show

$$T_i = \begin{bmatrix} \dot{x} \\ \Omega \\ \Omega_i \end{bmatrix}^T \mathbf{J}_i(R, Q_i) \begin{bmatrix} \dot{x} \\ \Omega \\ \Omega_i \end{bmatrix}.$$

where the configuration-dependent inertia for $\mathcal{B}_i$, namely $\mathbf{J}_i(R, Q_i) \in \mathbb{R}^{9\times9}$ is

$$\mathbf{J}_i(R, Q_i) = \begin{bmatrix} m_i I_{3\times3} & -m_i R(\hat{\mu}_i + \widehat{Q_i\nu_i}) & -m_i RQ_i\hat{\nu}_i \\ m_i(\hat{\mu}_i + \widehat{Q_i\nu_i})R^T & m_i\hat{\mu}_i^T\hat{\mu}_i + Q_iJ_iQ_i^T + m_i(\hat{\mu}_i^T\widehat{Q_i\nu_i} + \widehat{Q_i\nu_i}^T\hat{\mu}_i) & Q_iJ_i + m_i\hat{\mu}_i^TQ_i\hat{\nu}_i \\ m_i\hat{\nu}_iQ_i^TR^T & J_iQ_i^T + m_i\hat{\nu}_i^TQ_i^T\hat{\mu}_i & J_i \end{bmatrix}. \tag{45}$$

From (40), the derivative of the inertia can be expressed with the following matrix $\mathbf{K}_i \in \mathbb{R}^{9\times9}$,

$$\mathbf{K}_i(R, Q_i, \Omega, \Omega_i) = \begin{bmatrix} 0 & m_iR((\hat{\mu}_i + \widehat{Q_i\nu_i})\Omega + Q_i\hat{\nu}_i\Omega_i)^\wedge & m_iR(-\hat{\Omega}Q_i\hat{\nu}_i + Q_i\widehat{\hat{\nu}_i\Omega_i}) \\ 0 & m_i(\hat{\mu}_i + \widehat{Q_i\nu_i})\widehat{R^T\dot{x}} & m_i\widehat{R^T\dot{x}}Q_i\hat{\nu}_i - Q_i(J_iQ_i^T\Omega)^\wedge + Q_iJ_i\widehat{Q_i^T\Omega} \\ & & -m_i\hat{\mu}_i\hat{\Omega}Q_i\hat{\nu}_i - m_i\widehat{\hat{\mu}_i\Omega}Q_i\hat{\nu}_i \\ & & -Q_i\widehat{J_i\Omega_i} + m_i\hat{\mu}_iQ_i\widehat{\hat{\nu}_i\Omega_i} \\ 0 & m_i\hat{\nu}_iQ_i^T\widehat{R^T\dot{x}} & m_i\hat{\nu}_i(Q_i^TR^T\dot{x})^\wedge + J_i\widehat{Q_i^T\Omega} - m_i\hat{\nu}(Q^T\hat{\mu}_i\Omega)^\wedge \end{bmatrix}. \tag{46}$$

The total kinetic energy is the sum of the contributions of the body, the wings and the abdomen, as given by

$$T = T_B + T_R + T_L + T_A. \tag{47}$$

Potential Energy The gravitational potential energy of the body is

$$U_B = -m_B g e_3^T x.$$

The gravitational potential energy of $\mathcal{B}_i$ is

$$U_i = -m_i g e_3^T (x + R\mu_i + RQ_i\nu_i).$$

The total potential energy is

$$U = U_B + U_R + U_L + U_A. \tag{48}$$

The negative derivatives of the potential energy, namely $\mathbf{f}_g \in \mathbb{R}^{15}$ corresponds to the gravitational force and moment given by

$$\mathbf{f}_g \triangleq -\mathsf{T}_e^* \mathsf{L}_g U = \begin{bmatrix} (m_B + m_R + m_L + m_A) g e_3 \\ m_R g (\mu_R + Q_R \nu_R)^\wedge R^T e_3 + m_L g (\mu_L + Q_L \nu_L)^\wedge R^T e_3 + m_A g (\mu_A + Q_A \nu_A)^\wedge R^T e_3 \\ m_R g \hat{\nu}_R (Q_R^T R^T e_3) \\ m_L g \hat{\nu}_L (Q_L^T R^T e_3) \\ m_A g \hat{\nu}_A (Q_A^T R^T e_3) \end{bmatrix}, \tag{49}$$

where the total mass is denoted by $m \in \mathbb{R}$,

$$m = m_B + m_R + m_L + m_A. \tag{50}$$

Virtual Work Consider an infinitesimal aerodynamic force $dF(\nu) \in \mathbb{R}^3$ acting at the location of $\nu \in \mathbb{R}^3$ of the wing or the abdomen. In the inertial frame, the location of the force is given by $x + R\mu_i + RQ_i\nu$. Thus, the corresponding virtual work due to the aerodynamic force is

$$\int_{\mathcal{B}_i} \delta(x + R\mu_i + RQ_i\nu) \cdot RQ_i dF(\nu) d\nu = (\delta x + R\hat{\eta}\mu_i) \cdot RQ_i \int_{\mathcal{B}_i} dF(\nu) + \eta_i \cdot \int_{\mathcal{B}_i} \nu \times dF(\nu).$$

Let the resultant aerodynamic force and the moment about the wing root or the joint connecting the abdomen be

$$F_i = \int_{\mathcal{B}_i} dF_i(\nu), \quad M_i = \int_{\mathcal{B}_i} \nu \times dF_i(\nu).$$

Also, let $\tau_i \in \mathbb{R}^3$ be the control torque exerted to the wing root or at the joint connecting the abdomen, resolved in the body-fixed frame. As it is an internal torque, there will be a reactive torque, namely $-\tau_i$ exerted to the body.

The total virtual work due to the aerodynamic force and the control torque can be written as

$$\begin{aligned} \delta\mathcal{W} &= \sum_{i \in \{R,L,A\}} \delta x \cdot RQ_i F_i + \eta \cdot (\mu_i \times Q_i F_i - \tau_i) + \eta_i \cdot (M_i + Q_i^T \tau_i) \\ &= (\mathbf{f}_a + \mathbf{f}_\tau) \cdot \xi, \end{aligned} \tag{51}$$

where $\mathbf{f}_a, \mathbf{f}_\tau \in \mathbb{R}^{15}$ denote the contributions of the aerodynamic forces and the control torque, respectively. They are given by

$$\mathbf{f}_a = \begin{bmatrix} RQ_R F_R + RQ_L F_L + RQ_A F_A \\ \hat{\mu}_R Q_R F_R + \hat{\mu}_L Q_L F_L + \hat{\mu}_A Q_A F_A \\ M_R \\ M_L \\ M_A \end{bmatrix}, \tag{52}$$

$$\mathbf{f}_\tau = \begin{bmatrix} 0 \\ -\tau_R - \tau_L - \tau_A \\ Q_R^T \tau_R \\ Q_L^T \tau_L \\ Q_A^T \tau_A \end{bmatrix}. \tag{53}$$

Euler–Lagrange Equations The inertia tensor for the complete flapping wing aerial vehicle, namely $\mathbf{J}_g(\xi) \in \mathbb{R}^{15\times 15}$ is written as

$$\mathbf{J}_g(\xi) = \begin{bmatrix} m_B I_{3\times 3} + \mathbf{J}_{R_{11}} + \mathbf{J}_{L_{11}} + \mathbf{J}_{A_{11}} & \mathbf{J}_{R_{12}} + \mathbf{J}_{L_{12}} + \mathbf{J}_{A_{12}} & \mathbf{J}_{R_{13}} & \mathbf{J}_{L_{13}} & \mathbf{J}_{A_{13}} \\ \cdot & J_B + \mathbf{J}_{R_{22}} + \mathbf{J}_{L_{22}} + \mathbf{J}_{A_{22}} & \mathbf{J}_{R_{23}} & \mathbf{J}_{L_{23}} & \mathbf{J}_{A_{23}} \\ \cdot & \cdot & \mathbf{J}_{R_{33}} & 0 & 0 \\ \cdot & \cdot & 0 & \mathbf{J}_{L_{33}} & 0 \\ \cdot & \cdot & 0 & 0 & \mathbf{J}_{A_{33}} \end{bmatrix}, \tag{54}$$

where the subscript ij refers to the 3×3, i, j-th block of the corresponding matrix, and the unspecified blocks are chosen such that $\mathbf{J}_g$ becomes symmetric. The derivatives of the inertia are expressed by the following matrix $\mathbf{K}_g \in \mathbb{R}^{15\times 15}$ according to (40),

$$\mathbf{K}_g = \begin{bmatrix} 0 & \mathbf{K}_{R_{12}} + \mathbf{K}_{L_{12}} + \mathbf{K}_{A_{12}} & \mathbf{K}_{R_{13}} & \mathbf{K}_{L_{13}} & \mathbf{K}_{A_{13}} \\ 0 & \mathbf{K}_{R_{22}} + \mathbf{K}_{L_{22}} + \mathbf{K}_{A_{22}} & \mathbf{K}_{R_{23}} & \mathbf{K}_{L_{23}} & \mathbf{K}_{A_{23}} \\ 0 & \mathbf{K}_{R_{32}} & \mathbf{K}_{R_{33}} & 0 & 0 \\ 0 & \mathbf{K}_{L_{32}} & 0 & \mathbf{K}_{L_{33}} & 0 \\ 0 & \mathbf{K}_{A_{32}} & 0 & 0 & \mathbf{K}_{A_{33}} \end{bmatrix}. \tag{55}$$

The co-adjoint operator corresponds to the following matrix,

$$\mathrm{ad}^*_\xi = \mathrm{diag}[0_{3\times 3}, -\hat{\Omega}, -\hat{\Omega}_R, -\hat{\Omega}_L, -\hat{\Omega}_A]. \tag{56}$$

The Euler–Lagrange equations are given according to (41) as

$$\mathbf{J}_g(\dot{\xi}) - \mathrm{ad}^*_\xi \cdot \mathbf{J}_g(\xi) + \mathbf{L}_g(\xi)\xi = \mathbf{f}_a + \mathbf{f}_g + \mathbf{f}_\tau. \tag{57}$$

The matrix $\mathbf{L}_g(\xi) = \mathbf{K}_g(\xi) - \frac{1}{2}\mathbf{K}_g^T(\xi) \in \mathbb{R}^{15\times 15}$ represents the effects of the dependency of the inertia on the configuration, and it is more explicitly given in the appendix.

The above Euler–Lagrange equations are driven by the control torque acting on the joint of the wings and the joint of the abdomen, and they can be simulated by any ODE solver with the initial condition $(g(0), \xi(0))$ and the trajectory of $(\tau_R(t), \tau_L(t), \tau_A(t))$.

C. Prescribed Wing Kinematics and Abdomen Attitude

In case the flapping motion of the wings and the relative motion of the abdomen are prescribed, i.e., $Q_R(t), Q_L(t), Q_A(t)$ are given as a function of time, a reduced set of equations for (x, R) can be constructed as follows.

Let the configuration variables be decomposed into two parts, $g = (g_1, g_2)$ and $\xi = (\xi_1, \xi_2)$ with

$$g_1 = (x, R), \quad \xi_1 = [\dot{x}, \Omega], \tag{58}$$

$$g_2 = (Q_R, Q_L, Q_A), \quad \xi_2 = [\Omega_R, \Omega_L, \Omega_A]. \tag{59}$$

According to the assumption $(g_2, \xi_2, \dot{\xi}_2)$ are already known. We construct differential equations for ξ_1 as follows. The Euler–Lagrange equation (57) can be decomposed accordingly as

$$\mathbf{J}_{11}\dot{\xi}_1 + \mathbf{J}_{12}\dot{\xi}_2 - \mathrm{ad}^*_{\xi_1} \cdot (\mathbf{J}_{11}\xi_1 + \mathbf{J}_{12}\xi_2) + \mathbf{L}_{11}\xi_1 + \mathbf{L}_{12}\xi_2 = \mathbf{f}_{a_1} + \mathbf{f}_{g_1} + \mathbf{f}_{\tau_1}, \tag{60}$$

$$\mathbf{J}_{21}\dot{\xi}_1 + \mathbf{J}_{22}\dot{\xi}_2 - \mathrm{ad}^*_{\xi_2} \cdot (\mathbf{J}_{21}\xi_1 + \mathbf{J}_{22}\xi_2) + \mathbf{L}_{21}\xi_1 + \mathbf{L}_{22}\xi_2 = \mathbf{f}_{a_2} + \mathbf{f}_{g_2} + \mathbf{f}_{\tau_2}, \tag{61}$$

where the matrices $\mathbf{J}_g, \mathbf{L} \in \mathbb{R}^{15\times 15}$ are decomposed after the first six rows and columns. For example, $\mathbf{J}_{11} \in \mathbb{R}^{6\times 6}$ is the first 6×6 diagonal block of $\mathbf{J}_g$, and the remaining parts of the first 6 rows are defined as $\mathbf{J}_{12} \in \mathbb{R}^{6\times 9}$. We cannot integrate (60) separately, as it is coupled with (61) through the unknown (τ_R, τ_L, τ_A).

From (53),

$$\mathbf{f}_{\tau_1} = \begin{bmatrix} 0 & 0 & 0 \\ -Q_R & -Q_L & -Q_A \end{bmatrix} \mathbf{f}_{\tau_2} \triangleq C\mathbf{f}_{\tau_2},$$

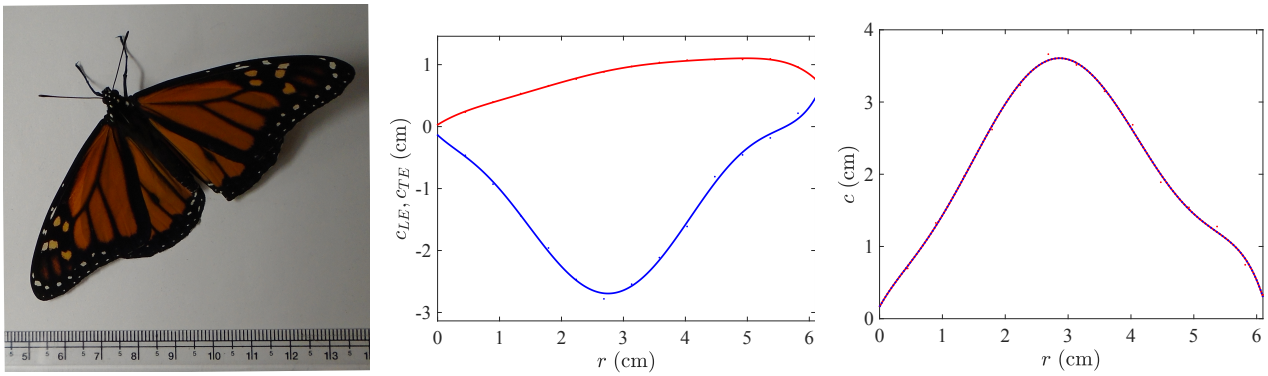

(a) Example butterfly specimen (b) Leading/Trailing edge $c_{LE}(r)$, $c_{TE}(r)$ (c) Chord $c(r)$

Fig. 9 Monarch wing shape and chord.

for $C(Q_R, Q_L, Q_A) \in \mathbb{R}^{6\times 9}$. Multiply C to (61), and subtract it from (60) to obtain

$$\begin{aligned}&(\mathbf{J}_{11} - C\mathbf{J}_{21})\dot{\xi}_1 - (\mathrm{ad}^*_{\xi_1}\mathbf{J}_{11} - C\mathrm{ad}^*_{\xi_2}\mathbf{J}_{21})\xi_1 + (\mathbf{L}_{11} - C\mathbf{L}_{21})\xi_1\\ &= -(\mathbf{J}_{12} - C\mathbf{J}_{22})\dot{\xi}_2 + (\mathrm{ad}^*_{\xi_1}\mathbf{J}_{12} - C\mathrm{ad}^*_{\xi_2}\mathbf{J}_{22})\xi_2 - (\mathbf{L}_{12} - C\mathbf{L}_{22})\xi_2\\ &\quad + \mathbf{f}_{a_1} + \mathbf{f}_{g_1} - C(\mathbf{f}_{a_2} + \mathbf{f}_{g_2}).\end{aligned} \tag{62}$$

Now, the unknown (τ_R, τ_L, τ_A) is eliminated, and for given $(g_2, \xi_2, \dot{\xi}_2)$ the above can be simulated to construct (g_1, ξ_1). Once (g_1, ξ_1) is obtained, it can be substituted into (61) to compute (τ_R, τ_L, τ_A) that the torque at the thorax required to rotate the wings and the abdomen as described.

D. Prescribed Wing Kinematics and Abdomen/Body Attitude

Next, we consider the case where the attitude of the thorax is prescribed additionally. As such all of $(R(t), Q_R(t), Q_L(t), Q_A(t))$ are given as a function of time. We construct a equation of motion for the position x.

The first block of (57) is written as

$$m\ddot{x} + \sum_{i\in\{R,L,A\}} \left\{\mathbf{J}_{i_{12}}\dot{\Omega} + \mathbf{J}_{i_{13}}\dot{\Omega}_i + \mathbf{K}_{i_{12}}\Omega + \mathbf{K}_{i_{13}}\Omega_i\right\} = R\sum_{i\in\{R,L,A\}} Q_i F_i + mge_3, \tag{63}$$

which can be numerically integrated to construct $(x, \dot{x})$. The corresponding control torque (τ_R, τ_L, τ_A) can be computed by (61).

V. Dynamic Simulation for Monarch Butterfly

A. Monarch Morphological Parameters

The wing shape and chord are determined from an example butterfly specimen shown in Fig. 9. The location of the leading edge and the trailing edge are measured along the span-wise direction, and they are fitted by sixth-order polynomials. The resulting measurements and the fitted curve are illustrated in Fig. 9. From the fitted chord, we determine the morphological dimensions related to the wing shown in Table 1. The mass of the wing and body segments and dimensions related to the butterfly body were calculated based on avergage values from six butterfly specimens and are shown in Table 1.

For the calculation of the inertia matrix, the head/thorax is considered as a cylinder with the height h_B and the diameter w_B. The moment of inertia of the body about its center of gravity is

$$J_B = m_B\,\mathrm{diag}[\frac{1}{8}w_B^2,\ \frac{1}{16}w_B^2 + \frac{1}{12}h_B^2,\ \frac{1}{16}w_B^2 + \frac{1}{12}h_B^2].$$

Table 1 Monarch parameters.

Head/Thorax		Abdomen		Right Wing	
m_B	1.485×10^{-4} kg	m_A	1.092×10^{-4} kg	m_R	2.5100×10^{-5} kg
h_B	1.463×10^{-2} m	h_A	1.738×10^{-2} m	$\bar{c}$	2.0905×10^{-2} m
w_B	5.680×10^{-3} m	w_A	3.710×10^{-3} m	l	6.0996×10^{-2} m
$J_{B_{xx}}$	5.9887×10^{-10} kgm^2	$J_{A_{xx}}$	1.8788×10^{-10} kgm^2	$J_{R_{xx}}$	2.7568×10^{-8} kgm^2
$J_{B_{yy}}$	2.9481×10^{-9} kgm^2	$J_{A_{yy}}$	1.1089×10^{-8} kgm^2	$J_{R_{xy}}$	2.4957×10^{-9} kgm^2
$J_{B_{zz}}$	2.9481×10^{-9} kgm^2	$J_{A_{zz}}$	1.1089×10^{-8} kgm^2	$J_{R_{yy}}$	2.5799×10^{-9} kgm^2
				$J_{R_{zz}}$	3.0148×10^{-8} kgm^2
				ν_{R_x}	-4.4378×10^{-3} m
				ν_{R_y}	1.5176×10^{-2} m
				S	1.2751×10^{-3} m^2
				$\mathcal{AR}$	2.9178
				$\tilde{r}_1$	4.9761×10^{-1}
				$\tilde{r}_2$	5.4332×10^{-1}
				$\tilde{r}_3$	5.8030×10^{-1}
				r_{cp}	6.5148×10^{-2} m
				$\tilde{v}$	1.2496
				$\tilde{r}_1(v)$	4.8750×10^{-1}
				$\tilde{r}_2(v)$	5.1653×10^{-1}
				r_{rot}	3.3383×10^{-2} m

(The properties of the left wing are identical to the right wing, except $\nu_{L_y} = -\nu_{R_y}$, $J_{L_{xy}} = -J_{R_{xy}}$.)

The abdomen is also considered as a cylinder. Its moment of inertia about the joint is

$$J_A = m_A \,\text{diag}[\frac{1}{8}w_A^2,\ \frac{1}{16}w_A^2 + \frac{1}{3}h_A^2,\ \frac{1}{16}w_B^2 + \frac{1}{3}h_A^2].$$

Next, the right wing is considered as a thin plate with a uniform, negligible thickness. The mass element is written as

$$dm = \frac{m_R}{S}dxdy,$$

where $\frac{m_R}{S}$ corresponds to the area density in the unit of kg/m^2. Thus, the mass center of the right wing is located at

$$\nu_{R_x} = \frac{1}{m_R}\int_{\mathcal{B}_R} x dm = \frac{1}{S}\int_0^l \int_{c_{TE}(y)}^{c_{LE}(y)} x dxdy = \frac{1}{S}\int_0^l \frac{1}{2}(c_{LE}^2(y) - c_{TE}^2(y))dy,$$
$$\nu_{R_y} = \frac{1}{m_R}\int_{\mathcal{B}_R} y dm = \frac{1}{S}\int_0^l \int_{c_{TE}(y)}^{c_{LE}(y)} y dxdy = \frac{1}{S}\int_0^l (c_{LE}(y) - c_{TE}(y))y dy.$$

Thus, the moment of inertia about the wing root is given by

$$J_{R_{xx}} = \int_{\mathcal{B}_R} y^2 dm = \frac{m_R}{S}\int_0^l \int_{c_{TE}(y)}^{c_{LE}(y)} y^2 dxdy = \frac{m_R}{S}\int_0^l y^2(c_{LE}(y) - c_{TE}(y))dy,$$
$$J_{R_{xy}} = \int_{\mathcal{B}_R} -xy dm = \frac{m_R}{S}\int_0^l \int_{c_{TE}(y)}^{c_{LE}(y)} -xy dxdy = \frac{m_R}{S}\int_0^l -\frac{1}{2}(c_{LE}^2(y) - c_{TE}^2(y))y dy,$$
$$J_{R_{yy}} = \int_{\mathcal{B}_R} x^2 dm = \frac{m_R}{S}\int_0^l \int_{c_{TE}(y)}^{c_{LE}(y)} x^2 dxdy = \frac{m_R}{S}\int_0^l \frac{1}{3}(c_{LE}^3(y) - c_{TE}^3(y))dy,$$
$$J_{R_{zz}} = J_{R_{xx}} + J_{R_{yy}}.$$

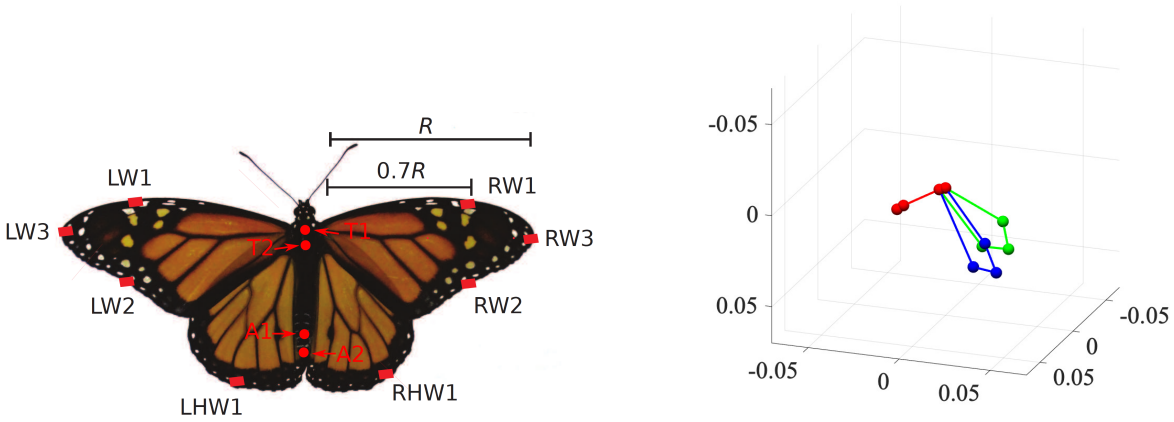

(a) Marker location

(b) Monarch object reconostructed by markers

Fig. 10 Monarch motion capture.

Similarly, for the left wing, we have

$$
\begin{aligned}
J_{L_{xx}} &= \frac{m_R}{S}\int_0^{-l}\int_{c_{TE}(-y)}^{c_{LE}(-y)} y^2 dxdy = J_{R_{xx}} \\
J_{L_{xy}} &= \frac{m_R}{S}\int_0^{-l}\int_{c_{TE}(-y)}^{c_{LE}(-y)} -xydxdy = -J_{R_{xy}} \\
J_{L_{yy}} &= \frac{m_R}{S}\int_0^{-l}\int_{c_{TE}(-y)}^{c_{LE}(-y)} x^2 dxdy = J_{R_{xx}} \\
J_{L_{zz}} &= J_{R_{zz}}.
\end{aligned}
$$

Finally, it is assumed that the root of the wing and the joint of the abdomen are located at

$$
\begin{aligned}
\mu_R &= [0,\ \frac{w_B}{2},\ 0], \\
\mu_L &= [0,\ -\frac{w_B}{2},\ 0], \\
\mu_A &= [-\frac{h_B}{2},\ 0,\ 0].
\end{aligned}
$$

B. Flight Characteristics of Monarch

The flight of an actual Monarch butterfly is studied by a motion capture system. The twelve markers are attached to a Monarch as illustrated in Fig. 10(a), and the position of each marker is measured by a VICON motion capture system at 200 Hz.

These are converted into (x, R, Q_R, Q_L, Q_A) as follows. It is considered that the origin of the body, namely x, is located at the center of T_1 and T_2. For the body attitude R, it is assumed that the first axis is along $T_1 - T_2$ and the second axis is parallel to the ground, i.e., there is no body roll. This is reasonable as the measured flight trajectory is almost straight. For the attitude of the abdomen, the first axis points from the center of A_1 and A_2 toward T_2, and the second axis is parallel to the ground. The resulting rotation matrix is left multiplied by R^T to obtain the relative attitude Q_A.

For the right wing attitude, it is assumed that the wing root is located at the center of T_1 and T_2. The wing plane always passes through the wing root exactly, and it is spanned by the three markers on the right wing. However, due to the measurement errors and the flexibility of the wing, those points do not exactly lie on a single plane. Instead, we find the normal vector of the plane such that the sum of the squared distance between each marker and the plane is minimized. The normal vector yields the third axis of $\mathcal{F}_R$. For the second axis, the vector from the wing root to RW_3

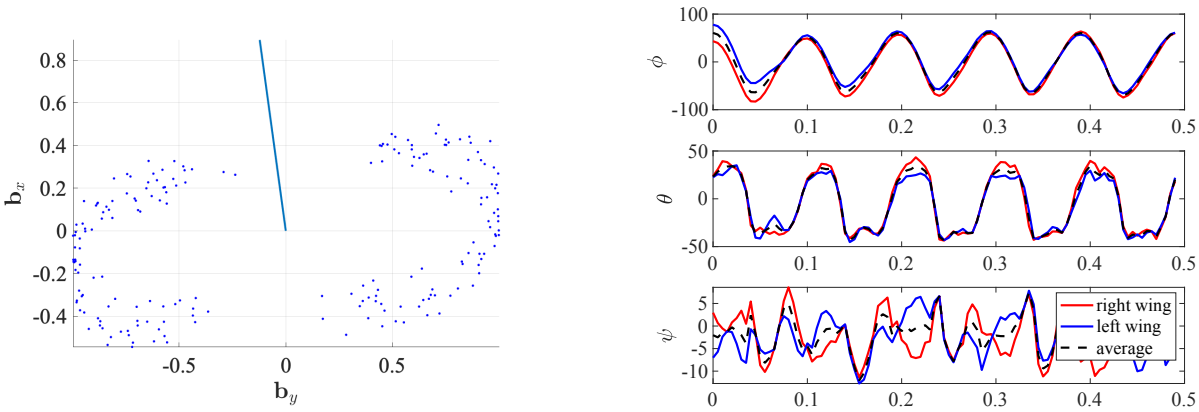

(a) wing tip locations

(b) wing kinematics angles

Fig. 11 Monarch wing kinematics. The wing kinematics angles are in degrees.

is projected on to the fitted plane. The first axis is determined by the cross product of the second axis and the third axis. These yield the rotation matrix of the right wing from the inertial frame, and by left multiplying R^T, we obtain Q_R. The attitude of the left wing, namely Q_L is constructed similarly.

Next, the computed $(Q_R(t), Q_L(t))$ are converted into wing kinematics angles as follows. First, we determine the wing stroke plane. In the absences of the deviation angle ψ, the second column of $Q_R(t)$ and $Q_L(t)$ over multiple time instances span the stroke plane. We find the stroke plane such that the sum of the squared distance for $Q_R(t)e_2$ and $Q_L(t)e_2$ for varying t over the experiment period is minimized. It turns out that the normal vector to the stroke plane is not in the $\mathbf{b}_x$–$\mathbf{b}_z$ plane. More explicitly, it is given by $[-0.8948, -0.1222, 0.4294]$, i.e., it is rotated by -7.77 deg when observed the dorsal side, or the right wing tip is ahead of the left wing tip (Fig. 11(a)). This might have been caused by the asymmetry of the particular Monarch butterfly used in the experiment, or the bias in the marker attachment. Instead of dealing with the asymmetry in the left wing and the right wing, we multiply $\exp(7.77\hat{e}_3)$ to Q_R and Q_L such that they become symmetric in the least square sense. The resulting normal vector of the stroke plane lies in the $\mathbf{b}_x$–$\mathbf{b}_z$ plane, and the stroke plane angle is $\beta = 25.42$ deg. From the given β, and rotated $Q_R(t), Q_L(t)$, we can determine the wing kinematics angles $(\phi_R(t), \theta_R(t), \psi_R(t)$, and $(\phi_L(t), \theta_L(t), \psi_L(t))$ according to (3) and (6), respectively. These are illustrated in Fig. 11(b). The wing kinematics angles for the right wing are mostly consistent with the the left wing, except the small deviation angle. Assuming the symmetric wing kinematics, we take the average between the right wing and the left wing, and they are fitted with Fourier series to be used in the subsequent dynamic simulation.

C. Dynamic Simulation

From the above wing kinematics angles and the body/abdomen attitude obtained by the actual Monarch butterfly, we numerically integrate the quasi-steady position dynamics, namely (63). The corresponding results are compared against the experimental data. These are illustrated in Fig. 12. In general, the downstrokes generate the lift upward, and the upstrokes generate thrust forward, while yielding a climbing trajectory with oscillation.

The proposed quasi-steady aerodynamic model generates greater lift and thrust, and consequently causing higher climb rate and forward velocity. However, it is consistent with the experimental data in a qualitative manner, thereby validating the proposed model.

D. Effects of Abdomen

It turns out that for Monarch butterfly flights, the abdomen oscillate at the same frequency of the wing flapping angle with the opposite phase, i.e., the abdomen rotates downward during the wing upstrokes.

To test the effects of abdomen undulation with the proposed model, we simulate the above Monarch model for 50 strokes while fixing the abdomen pitching angle to the averaged value. These results are illustrated at Fig. 13. While the difference is not substantial, it is shown that the abdomen undulation slightly increases the climb rate and the forward velocity.

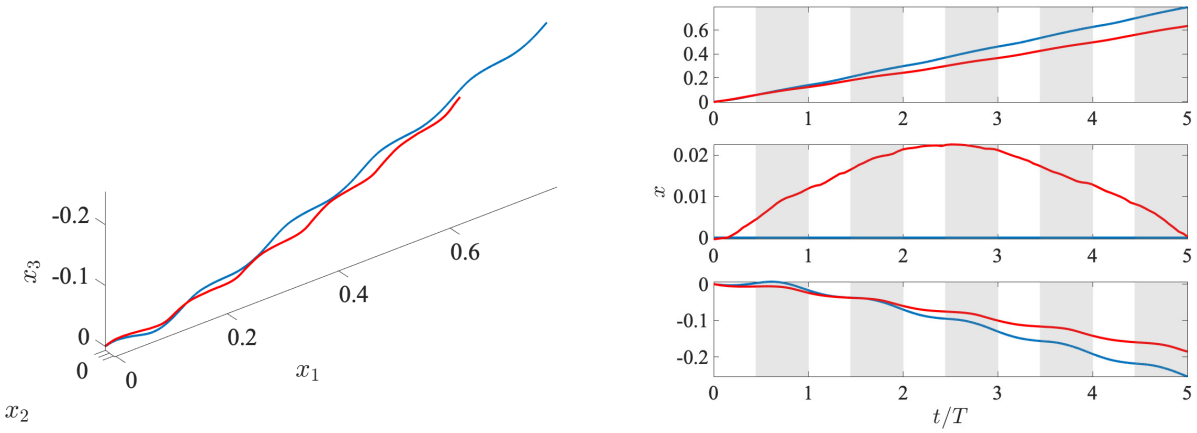

(a) Position trajectory

(b) Position x

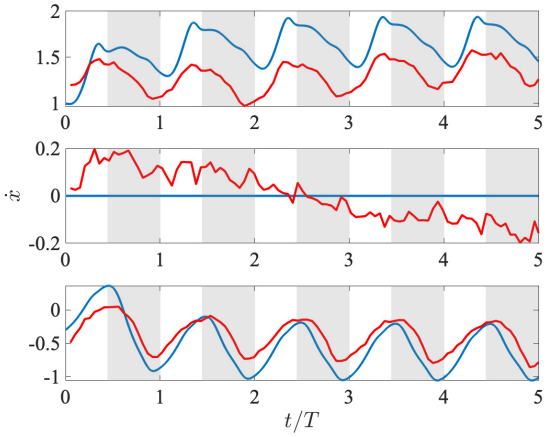

(c) Velocity $\dot{x}$

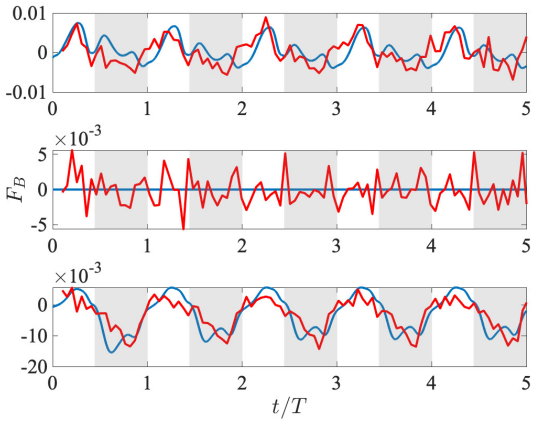

(d) Resultant force in the body-fixed frame

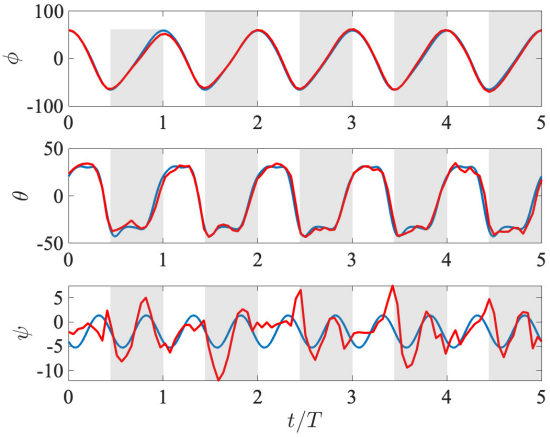

(e) Wing kinematics angles

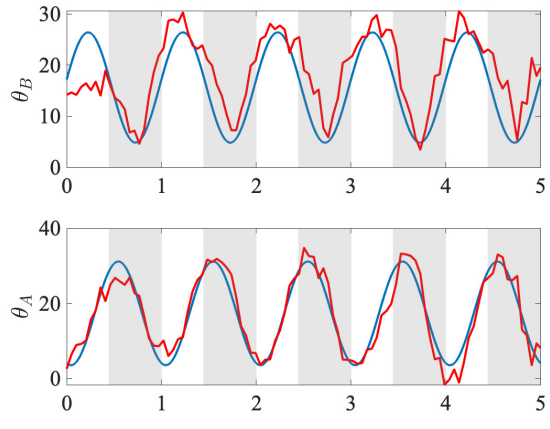

(f) Body pitch / Abdomen relative pitch

Fig. 12 Comparison between the QS model (blue) and the experimental data (red); shaded area corresponds to downstroke; the resultant force of the experiment is constructed by the acceleration of the thorax, multiplied by the total mass and subtracted by the gravity. The position is shown in m, velocity in m/s, forces in N, and angles in degrees.

Furthermore, we consider another case when the abdomen undulate in the opposite phase to the measured vales. Interestingly, this yields the worst results, where the forward velocity and the climb rate are smaller than the case of fixed abdomen. This suggests that the abdomen undulation has a coupling effect to the translational dynamics of the thorax, as represented by the additional force in (63),

$$-\mathbf{J}_{A_{13}}\dot{\Omega}_A - \mathbf{K}_{A_{13}}\Omega_A.$$

It is interesting to notice that the Monarch butterfly undulates its abdomen such that the above terms become beneficial to the flight.

E. Asymptotic Stability

Another interesting results of Fig. 13(c) is that the trajectory of the velocity asymptotically converges to a periodic orbit, while the initial condition does not belong to the periodic orbit exactly. This suggests that the flapping motion captured by the Monarch butterfly yields an asymptotically stable periodic solution. This should be further investigated by dynamic system theory such as Floquet's theorem.

VI. Conclusions

This paper presents a dynamic model for a flapping wing aerial vehicle that can characterize the flight of a butterfly. It is composed of articulated rigid bodies such that the dynamic effects of the inertial coupling between multiple parts can be studied. A quasi-steady aerodynamic model is also constructed without assuming that the flapping frequency is sufficiently large. Consequently, the proposed model is particularly useful for the butterfly flight that is characterized by relatively large wings flapping at a low frequency and body/abdomen undulation coupled with the flapping motion.

This proposed model is compared with the data obtained by a live Monarch butterfly. It is shown that the abdomen undulation increases the flight velocity, and the flapping of the Monarch butterfly yields an asymptotically stable periodic orbit. For future study, the effects of the abdomen undulation should be quantitatively evaluated to compare its undulation, and the stability should be rigorously analyzed.

Appendix

A. Effects of Configuration-Dependency in Inertia

$$\mathbf{L}_g = \begin{bmatrix} 0 & \mathbf{K}_{R_{12}} + \mathbf{K}_{L_{12}} + \mathbf{K}_{A_{12}} & \mathbf{K}_{R_{13}} & \mathbf{K}_{L_{13}} & \mathbf{K}_{A_{13}} \\ -\frac{1}{2}(\mathbf{K}_{R_{12}} + \mathbf{K}_{L_{12}} + \mathbf{K}_{A_{12}})^T & \mathbf{K}_{R_{22}} + \mathbf{K}_{L_{22}} + \mathbf{K}_{A_{22}} - \frac{1}{2}(\mathbf{K}_{R_{22}} + \mathbf{K}_{L_{22}} + \mathbf{K}_{A_{22}})^T & \mathbf{K}_{R_{23}} - \frac{1}{2}\mathbf{K}_{R_{32}}^T & \mathbf{K}_{L_{23}} - \frac{1}{2}\mathbf{K}_{L_{32}}^T & \mathbf{K}_{A_{23}} - \frac{1}{2}\mathbf{K}_{A_{32}}^T \\ -\frac{1}{2}\mathbf{K}_{R_{13}}^T & \mathbf{K}_{R_{32}} - \frac{1}{2}\mathbf{K}_{R_{23}}^T & \mathbf{K}_{R_{33}} - \frac{1}{2}\mathbf{K}_{R_{33}}^T & 0 & 0 \\ -\frac{1}{2}\mathbf{K}_{L_{13}}^T & \mathbf{K}_{L_{32}} - \frac{1}{2}\mathbf{K}_{L_{23}}^T & 0 & \mathbf{K}_{L_{33}} - \frac{1}{2}\mathbf{K}_{L_{33}}^T & 0 \\ -\frac{1}{2}\mathbf{K}_{A_{13}}^T & \mathbf{K}_{A_{32}} - \frac{1}{2}\mathbf{K}_{A_{23}}^T & 0 & 0 & \mathbf{K}_{A_{33}} - \frac{1}{2}\mathbf{K}_{A_{33}}^T \end{bmatrix}. \tag{64}$$

B. Open-Source Software Package

A software package for the proposed quasi-state dynamic model has been developed in Matlab, and it is shared as an open-source library at `https://github.com/fdcl-gwu/FWUAV`.

This is composed of the following components.

- Morphological parameters of Monarch butterfly are defied at `morp_MONARCH.m`
- The raw data from VICON are processed by the following three files under `/exp_data`.

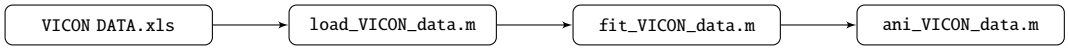

- For given torque at the wing and the abdomen, the complete dynamics (57) are simulated as follows.

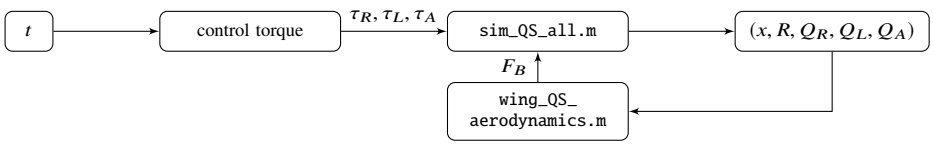

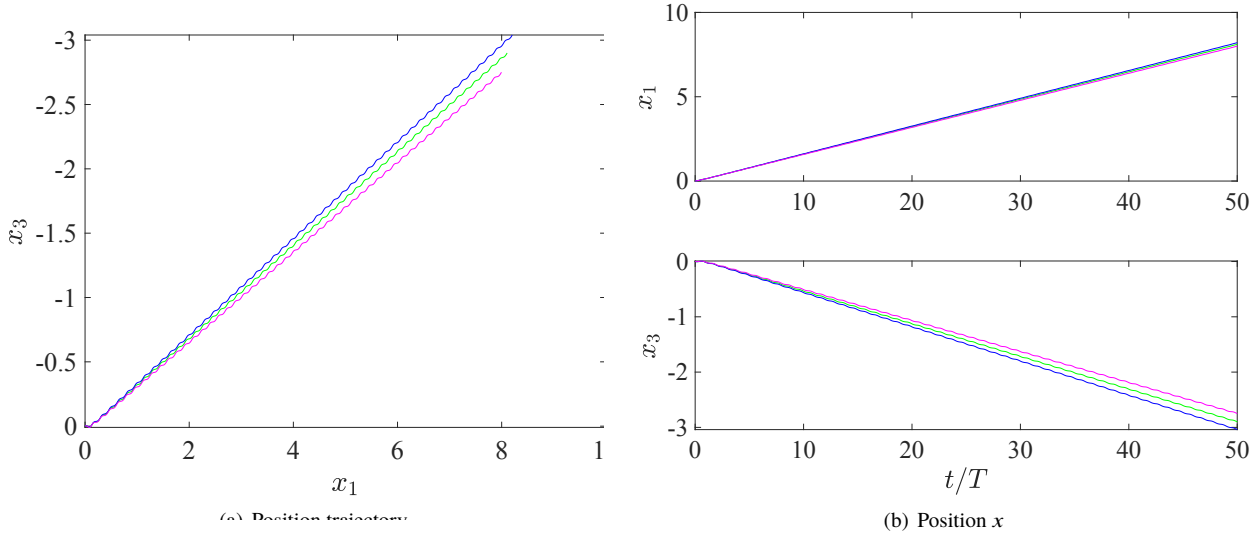

(a) Position trajectory (b) Position x

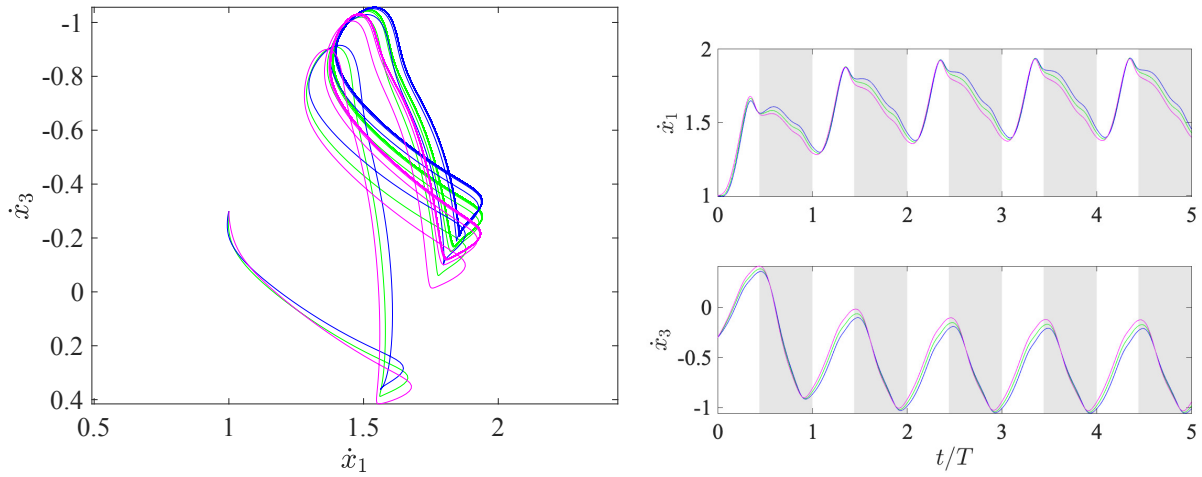

(c) Velocity trajectory (d) Velocity $\dot{x}$ (for the first 5 strokes)

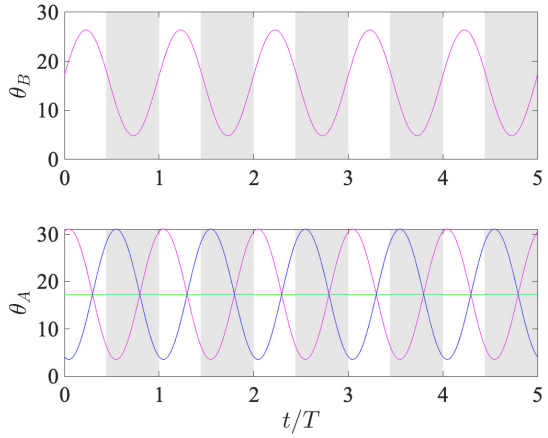

(e) thorax pitch / abdomen pitch (for the first 5 strokes)

Fig. 13 Comparison between flight with abdomen undulation (blue), without abdomen undulation (green), with abdomen undulation in the opposite phase (purple); the simulation is for 50 strokes, and the results of the first 5 strokes are illustrated for the subfigure (d) and (e). The position is shown in m, velocity in m/s, and angles in degrees.

- For given wing Euler angles and the abdomen attitude, the position and the attitude dynamics of the thorax, namely (62) are simulated as follows.

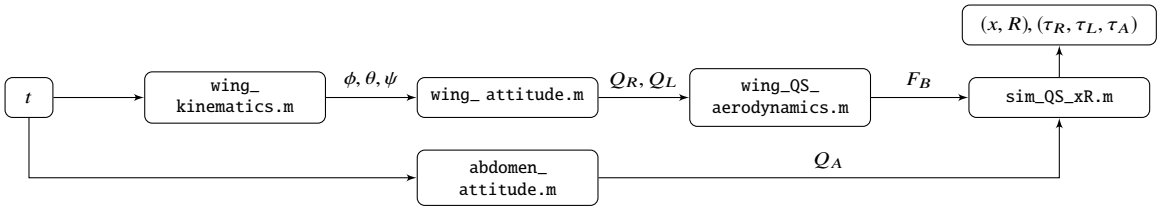

- For given wing Euler angles, the thorax attitude, and the abdomen attitude, the position dynamics (63) are simulated as follows.

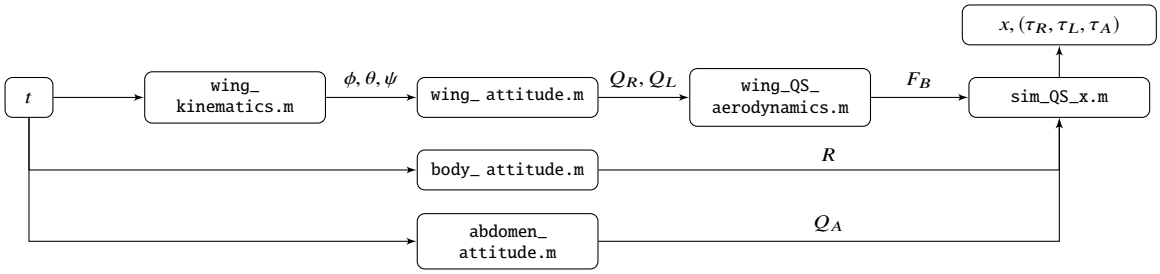

Acknowledgments

This research has been supported in parts by NSF CMMI-1761618 and NSF CMMI-1760928.

References

[1] Brower, L., "Monarch Migration," *Natural History*, Vol. 85, No. 6, 1977.

[2] Brower, L., "Monarch butterfly orientation: missing pieces of a magnificent puzzle," *The Journal of experimental biology*, Vol. 199, 1996, pp. 93–103. URL http://www.ncbi.nlm.nih.gov/pubmed/9317405.

[3] Masters, A. R., Malcolm, S. B., and Brower, L. P., "Monarch Butterfly (Danaus Plexippus) Thermoregulatory Behavior and Adaptations for Overwintering in Mexico," *Ecology*, Vol. 69, No. 2, 1988, p. 458. doi:10.2307/1940444, URL http://www.jstor.org/stable/1940444?origin=crossref.

[4] Merlin, C., Gegear, R. J., and Reppert, S. M., "Antennal Circadian Clocks Coordinate Sun Compass Orientation in Migratory Monarch Butterflies," *Science*, Vol. 325, No. 5948, 2009, pp. 1700–1704. doi:10.1126/science.1176221, URL http://www.sciencemag.org/cgi/doi/10.1126/science.1176221.

[5] Gibo, D. L., "Altitudes Attained By Migrating Monarch Butterflies, Danaus P. Plexippus (Lepidoptera: Danainae), as Reported By Glider Pilots," *Canadian Journal of Zoology*, Vol. 59, 1981, pp. 571–572.

[6] Srygley, R. B., Dudley, R., Oliveira, E. G., and Riveros, A. J., "El Niño, Host Plant Growth, and Migratory Butterfly Abundance in a Changing Climate," *Biotropica*, Vol. 46, No. 1, 2014, pp. 90–97. doi:10.1111/btp.12081.

[7] Templin, R. J., "Spectrum of animal flight: Insects to pterosaurs," *Progress in Aerospace Sciences*, Vol. 36, No. 5, 2000, pp. 393–436. doi:10.1016/S0376-0421(00)00007-5.

[8] Dickinson, M. H., Lehmann, F.-O., and Sane, S. P., "Wing rotation and the aerodynamic basis of insect flight," *Science*, Vol. 284, No. 5422, 1999, pp. 1954–1960. doi:10.1126/science.284.5422.1954, URL http://www.ncbi.nlm.nih.gov/pubmed/10373107http://www.sciencemag.org/content/284/5422/1954.short.

[9] Muijres, F. T., Elzinga, M. J., Melis, J. M., and Dickinson, M. H., "Flies Evade Looming Targets by Executing Rapid Visually Directed Banked Turns," *Science*, Vol. 344, No. 6180, 2014, pp. 172–177. doi:10.1126/science.1248955, URL http://www.sciencemag.org/content/344/6180/172.abstracthttp://www.sciencemag.org/cgi/doi/10.1126/science.1248955.

[10] Dillon, M. E., and Dudley, R., "Surpassing Mt. Everest: extreme flight performance of alpine bumble-bees." *Biology letters*, Vol. 10, 2014, p. 20130922. doi:10.1098/rsbl.2013.0922, URL http://www.ncbi.nlm.nih.gov/pubmed/24501268.

[11] Mountcastle, A. M., and Combes, S. A., "Wing flexibility enhances load-lifting capacity in bumblebees," *Proceedings of the Royal Society B*, Vol. 280, No. 1759, 2013, pp. 20130531–20130531. doi:10.1098/rspb.2013.0531, URL http://rspb.royalsocietypublishing.org/cgi/doi/10.1098/rspb.2013.0531.

[12] Wang, Z. J., "Dissecting Insect Flight," *Annual Review of Fluid Mechanics*, Vol. 37, No. 1, 2005, pp. 183–210. doi:10.1146/annurev.fluid.36.050802.121940, URL http://www.annualreviews.org/doi/abs/10.1146/annurev.fluid.36.050802.121940http://arjournals.annualreviews.org/doi/abs/10.1146/annurev.fluid.36.050802.121940.

[13] Jongerius, S. R., and Lentink, D., "Structural Analysis of a Dragonfly Wing," *Experimental Mechanics*, Vol. 50, No. 9, 2010, pp. 1323–1334. doi:10.1007/s11340-010-9411-x, URL http://link.springer.com/10.1007/s11340-010-9411-x.

[14] Wang, Z., "High-order methods for the Euler and Navier–Stokes equations on unstructured grids," *Progress in Aerospace Sciences*, Vol. 43, No. 1-3, 2007, pp. 1–41. doi:10.1016/j.paerosci.2007.05.001, URL http://linkinghub.elsevier.com/retrieve/pii/S0376042107000450.

[15] Alexander, D. E., "Unusual phase relationships between the forewings and hindwings in flying dragonflies," *Journal of Experimental Biology*, Vol. 109, No. 1, 1984, pp. 379–383.

[16] Wang, J. K., and Sun, M., "A computational study of the aerodynamics and forewing-hindwing interaction of a model dragonfly in forward flight," *Journal of Experimental Biology*, Vol. 208, No. 19, 2005, pp. 3785–3804. doi:10.1242/jeb.01852, URL http://jeb.biologists.org/cgi/doi/10.1242/jeb.01852.

[17] Shyy, W., Aono, H., Kang, C.-k., and Liu, H., *An Introduction to Flapping Wing Aerodynamics*, Cambridge University Press, New York, New York, 2013.

[18] Betts, C. R., and Wootton, R. J., "Wing Shape and Flight Behaviour in Butterflies (Lepidoptera: Papilionoidea and Hesperioidea): A Preliminary Analysis," *Journal of Experimental Biology*, Vol. 138, No. 1, 1988, pp. 271–288. URL http://jeb.biologists.org/content/138/1/271.abstract.

[19] Dudley, R., "Biomechanics of flight in neotropical butterflies: aerodynamics and mechanical power requirements," *Journal of experimental biology*, Vol. 357, No. 1, 1991, pp. 335–357. URL http://jeb.biologists.org/content/159/1/335.short.

[20] Thomas, A. L. R., Taylor, G. K., Srygley, R. B., Nudds, R. L., and Bomphrey, R. J., "Dragonfly flight: free-flight and tethered flow visualizations reveal a diverse array of unsteady lift-generating mechanisms, controlled primarily via angle of attack," *Journal of Experimental Biology*, Vol. 207, No. 24, 2004, pp. 4299–4323. doi:10.1242/jeb.01262, URL http://jeb.biologists.org/cgi/doi/10.1242/jeb.01262.

[21] Srygley, R. B., "Locomotor Mimicry in Butterflies? The Associations of Positions of Centres of Mass among Groups of Mimetic, Unprofitable Prey," *Philosophical Transactions of the Royal Society of London B: Biological Sciences*, Vol. 343, No. 1304, 1994, pp. 145–155. URL http://rstb.royalsocietypublishing.org/content/343/1304/145.abstract.

[22] Dudley, R., and Srygley, R., "Flight Physiology of Neotropical Butterflies: Allometry of Airspeeds During Natural Free Flight," *The Journal of experimental biology*, Vol. 191, No. 1, 1994, pp. 125–39. URL http://jeb.biologists.org/content/191/1/125.long.

[23] Lin, T., Zheng, L., Hedrick, T., and Mittal, R., "The significance of moment-of-inertia variation in flight manoeuvres of butterflies," *Bioinspiration & Biomimetics*, Vol. 7, No. 4, 2012, p. 044002. doi:10.1088/1748-3182/7/4/044002.

[24] Kang, C.-k., Cranford, J., Sridhar, M. K., Kodali, D., Landrum, D. B., and Slegers, N., "Experimental Characterization of a Butterfly in Climbing Flight," *AIAA Journal*, Vol. 56, No. 1, 2018, pp. 15–24. doi:10.2514/1.j055360, doi:10.2514/1.j055360.

[25] Tanaka, H., and Shimoyama, I., "Forward flight of swallowtail butterfly with simple flapping motion." *Bioinspiration & biomimetics*, Vol. 5, No. 2, 2010, p. 026003. doi:10.1088/1748-3182/5/3/039801.

[26] Elzinga, M. J., van Breugel, F., and Dickinson, M. H., "Strategies for the stabilization of longitudinal forward flapping flight revealed using a dynamically-scaled robotic fly," *Bioinspiration & biomimetics*, Vol. 9, 2015, p. 025001.

[27] Taha, H. E., Hajj, M. R., and Nayfeh, A. H., "Flight dynamics and control of flapping-wing MAVs: a review," *Nonlinear Dynamics*, Vol. 70, No. 2, 2012, pp. 907–939. doi:10.1007/s11071-012-0529-5, URL http://link.springer.com/10.1007/s11071-012-0529-5.

[28] Schenato, L., "Analysis and control of flapping flight: from biological to robotic insects," Phd dissertation, University of California, Berkeley, 2003.

[29] Xinyan Deng, Schenato, L., Wei Chung Wu, Sastry, S., Deng, X., Schenato, L., Wu, W. C., and Sastry, S., "Flapping flight for biomimetic robotic insects: part I-system modeling," *IEEE Transactions on Robotics*, Vol. 22, No. 4, 2006, pp. 776–788. doi:10.1109/TRO.2006.875480, URL http://ieeexplore.ieee.org/lpdocs/epic03/wrapper.htm?arnumber=1668260.

[30] Doman, D. B., Oppenheimer, M. W., and Sigthorsson, D. O., "Wingbeat Shape Modulation for Flapping-Wing Micro-Air-Vehicle Control During Hover," *Journal of Guidance, Control, and Dynamics*, Vol. 33, No. 3, 2010, pp. 724–739. doi:10.2514/1.47146, URL http://arc.aiaa.org/doi/abs/10.2514/1.47146.

[31] Shyy, W., Kang, C.-k., Chirarattananon, P., Ravi, S., and Liu, H., "Aerodynamics, sensing and control of insect-scale flapping-wing flight," *Proceedings of the Royal Society A: Mathematical, Physical and Engineering Science*, Vol. 472, No. 2186, 2016, p. 20150712. doi:10.1098/rspa.2015.0712, URL http://rspa.royalsocietypublishing.org/lookup/doi/10.1098/rspa.2015.0712.

[32] Sridhar, M., Kang, C.-K., and Landrum, D. B., "Beneficial Effect of the Coupled Wing-Body Dynamics on Power Consumption in Butterflies," *AIAA Scitech 2019 Forum*, AIAA 2019-0566, 2019. doi:10.2514/6.2019-0566.

[33] Yokoyama, N., Senda, K., Iima, M., and Hirai, N., "Aerodynamic forces and vortical structures in flapping butterfly's forward flight," *Physics of Fluids*, Vol. 25, No. 2, 2013, p. 021902. doi:10.1063/1.4790882, URL http://scitation.aip.org/content/aip/journal/pof2/25/2/10.1063/1.4790882.

[34] Jayakumar, J., Senda, K., and Yokoyama, N., "Control of Pitch Attitude by Abdomen During Forward Flight of Two-Dimensional Butterfly," *Journal of Aircraft*, Vol. 55, No. 6, 2018, pp. 2327–2337. doi:10.2514/1.c034767.

[35] Dyhr, J. P., Morgansen, K. A., Daniel, T. L., and Cowan, N. J., "Flexible strategies for flight control: an active role for the abdomen," *Journal of Experimental Biology*, Vol. 216, No. 9, 2013, pp. 1523–1536.

[36] Berman, G. J., and Wang, Z. J., "Energy-minimizing kinematics in hovering insect flight," *Journal of Fluid Mechanics*, Vol. 582, 2007, pp. 153–168.

[37] Ellington, C. P., "The aerodynamics of hovering insect flight. I. The quasi-steady analysis," *Philosophical Transactions of the Royal Society of London. B, Biological Sciences*, Vol. 305, No. 1122, 1984, pp. 1–15.

[38] Sane, S. P., and Dickinson, M. H., "The aerodynamic effects of wing rotation and a revised quasi-steady model of flapping flight," *Journal of experimental biology*, Vol. 205, No. 8, 2002, pp. 1087–1096.

[39] Lee, T., Leok, M., and McClamroch, N., *Global Formulation of Lagrangian and Hamiltonian Dynamics on Manifolds*, Springer, 2018. doi:10.1007/978-3-319-56953-6.